MICROFLUIDIC GENERATION OF POLYMERIC MICROPARTICLE DROPLETS

By

Blake F. Hanan

Thesis

Submitted to the Faculty of the

Graduate School of Vanderbilt University

in fulfillment of the requirements

for the degree of

Masters of Science

in

Biomedical Engineering

August 12, 2022

Nashville, Tennessee

Approved:

Craig Duvall, Ph.D.

Todd Giorgio, Ph.D.

ACKNOWLEDGMENTS

I would like to first thank Dr. Craig Duvall for the support, and accepting this project at an uncertain time in the world. This decision has made a profound impact on the trajectory of my life, career goals, and level of fulfillment. The lab you built is an intellectual powerhouse with an incredible support system, and I am looking forward to following the continued contributions you make to science, and the world.

Thank you to Carlisle DeJulius for your patience, mentorship, hard work, and attention to detail. You are a wonderful role model both personally and professionally; thank you showing me what it means to be a good scientist. I will always remember the advice, "perfect is the enemy of good." I think the reader will come to see that at times this was well embraced (if not *too* well), and other times, completely ignored.

Additionally, thank you to Dr. Marija Zanic, Dr. Beth Lawrence, and the Zanic Lab for introducing me to the world of biomaterials, microfluidics, and research as a whole. I wish you all continued success in the plight to understand the fascinating system that is the cytoskeleton, and in developing innovative engineering strategies to answer these questions.

This work would not have been possible without the VINSE staff and faculty, notably for the financial support in the form of a pilot grant to explore some of these methods freely. Additionally, a special thank you to Dr. Christina McGahan and Mike Valenti for the countless hours of trainings, troubleshooting, and long days in the cleanroom. Thank you to VINSE Tech Crew and Super Users, notably Alberto Esteban Linares, whose infinite tips and tricks, and healthy amount of cynicism, allowed me to overcome setbacks. Thank you for teaching me "recipe optimization is an art, not a science."

Finally, thank you to Chrissy Marasco, Jon Ehrman, John Wikswo and all the other SyBBURE folks for the years of mentoring, financial support, freedom to explore interesting problems, and allowing me to "do cool stuff". This is an incredibly special program responsible for a large amount of my growth, and some of my most fond memories of my time at Vanderbilt.

Thank you Mom, Dad, and Austin.

TABLE OF CONTENTS

Page

List of Figures

Chapter 1

Introduction and Significance

1.1 Innovation and Motivation

Long-term, sustained drug release utilizing an injectable delivery vehicle in localized, chronic diseases is a therapeutic strategy with the potential to extend the action of drugs, reduce drug off-target side effects, and improve patient compliance/outcomes[1]. Clinically approved systems are based on hydrolytically degradable poly(lactic-co-glycolic acid) (PLGA) microparticles (MPs) such as the osteoarthritis drug Zilretta[2]. However, the acidic breakdown products of PLGA can worsen inflammation[3], and bulk PLGA materials can elicit a foreign-body response[4]. An alternative is a polymeric MP which is oxidatively degradable. Reactive oxygen species (ROS)-responsive materials chemically scavenge ROS in oxidative environments and have been shown to have a therapeutic effect on ROS-driven pathologies[5,6]. In this way, antioxidant MPs exhibit disease-responsive drug release and can contribute to favorable therapeutic outcomes, unlike PLGA. Previous work in our laboratory has shown that MPs comprising poly(propylene sulfide) (PPS) scavenge ROS at the backbone thioether groups, in osteoarthritis, diabetic peripheral arterial disease, and traumatic optic neuropathy[5,6].

PPS MPs are limited to 5 μm and below due to the polymer's amorphous nature. More crystalline polysulfides can be used to generate larger MPs, and they are generated by a bulk emulsification process, however, this process results in high size dispersity and low drug loading. Droplet based emulsion microfluidic systems can be employed to improve upon these metrics[7–10], however most in-house methods used to fabricate these devices involve molding and casting polydimethylsiloxane (PDMS)[11], which swells in the presence of organic solvents[12]. Unfortunately, these aggressive solvents are necessary to solubilize current formulations of crystalline polysulfides and perform the emulsion. Because the geometry of the junction where the two fluid phases meet governs particle size[13,14], and these solvents change the geometry, there

is a need for a more solvent resistant microfluidic device material to ensure monodispersity.

The objective of this work is to develop an in-house fabrication method for a solvent-compatible droplet microfluidic device to manufacture antioxidant MPs out of a more crystalline polysulfide. MPs made with the new polysulfide polymer in a high-quality, solvent resistant droplet microfluidic device should generate larger-size MPs in higher quantities, with a narrow size dispersity, and highly efficient drug loading.

1.2 Specific Aims

The overall goal of this project is to reliably fabricate a versatile, solvent compatible droplet microfluidic device that generates large, monodisperse polymeric microparticles for drug encapsulation. **The hypothesis is that particle batches produced by the device will result in lower polydispersity indices over benchtop emulsion formulations.**

Aim 1: Design and fabricate a solvent compatible, high fidelity, droplet microfluidic device:

The first aim of this thesis is to understand how to microfabricate microfluidic channels into a substrate made of a solvent resistant material, i.e., glass. The general strategy employed was to start with a glass slide, pattern onto the surface a protective mask such that when the sample is placed in a chemical etchant, only the regions exposed will be etched, thus forming microchannels in the desired geometry. A recipe was developed that uses a sacrificial lift-off resist layer to selectively deposit a hard metal mask onto the surface of the glass, and the resulting samples are etched with microchannels. Various patterning materials and methods, layer thicknesses, substrate materials, and etchant concentrations were evaluated and optimized for their ability to withstand the etchant, avoid off target etching, and minimize defects. Channel profiles were measured to ensure high resolution, correct aspect ratios, and fidelity to the original design. Channel surface topology was similarly measured to verify etched surfaces are flat and high quality to prevent turbulent fluid flow and droplet breakup.

Aim 2: Demonstrate improvements in monodispersity of microfluidic generated polymeric microparticles over bulk emulsions:

The second aim of this thesis is to use these microfabricated chips to generate polymeric microparticles, and observe differences in quality metrics as compared to the bulk emulsion formulation. Bonding methods for sealing the microchannels were evaluated by checking for the presence of fluid outside of the channels. Thermal and adhesive bonding methods proved to be unsuccessful, however, PDMS capping sealed the channels well and was relatively solvent resistant. These devices, when two immiscible phases were introduced, promoted droplet formation of the water phase. However, given the goal of making polymeric microparticles loaded in the oil phase, the reverse emulsion was necessary. This was accomplished by modifying the surface of the channels to be more hydrophilic, ultimately with a novel polymeric zwitterionic silane, such that the water phase had a higher affinity for the walls of the channels and became the continuous phase. PLGA microparticles were successfully generated using the device and demonstrated preliminary improvements in quality metrics, notably the polydispersity index (PDI). Additionally, a crystalline polysulfide microparticle formulation was generated microfluidically, and demonstrated good quality metrics.

1.3 Outline

This thesis focuses on the optimization of a glass microfabrication recipe, and a leveraging of the resulting microfluidic devices to produce polymeric microparticles with better quality metrics. Chapter 2 provides an overview of microfluidics as a field and how to fabricate microfluidic devices. Chapter 3 discusses the microfabrication protocol developed for producing high-fidelity glass microfluidic devices, and metrics for success during the optimization of each step. Chapter 4 demonstrates a use case for this glass etching protocol by using a glass microfluidic device to generate oil-in-water droplets. These will form polymeric microparticles, and demonstrate better quality metrics as compared to the bulk emulsion formulation. Chapter 5 summarizes and discusses the impact of this work as a whole, considers future directions for this project, and enumerates potential challenges for scaling and translating this system to other polymers. Each experimental chapter consists of a brief introductory section followed by the methods, results, and

discussion.

Chapter 2

Background

2.1 Microfluidics

The mechanisms engineered by nature to control biological systems exists at incredibly small scales. The benchmark for reaching a good understanding of these systems is the ability to recreate them. Thus, our models, experiments, diagnostics, and therapies must include the same intentional design parameters that nature employs at the micro-level to develop and regulate function at these scales. The field of microfluidics is the practice of controlling fluids at a very small scale, often in devices with channels on the scale of micrometers, and offers many solutions in the realm of investigating and controlling biological systems, as well as automating biological and chemical processes.

The advantage of microfluidic technologies is in the ability to control device features with very high precision. These "chips" incorporate very intricate channels, allowing researchers to compartmentalize and automate complicated biochemical processes. The small channel sizes tend to be beneficial in that smaller quantities of samples and reagents are required to accomplish a process with high resolution and sensitivity, while decreasing the analysis time[15]. Physically, small channels sizes allow for laminar flow, which proves useful in many applications as the mixing of fluids (traditionally due to turbulent flow), is only present when intentionally included in the device design[16].

Although this technology has been available for over 2 decades now, it is ever improving, creating immense potential for new applications across research fields and therapeutic areas. Microfluidics can be used to create higher quality models than standard cell culture[17], high throughput screening for drug development[18,19], diagnostic tools[20], and the focus of this thesis, automation of lab work for improved efficiency, or lab-on-a-chip technology[21].

2.2 Principles of Microfabrication

Microchannels for microfluidics can be fabricated using two strategies: by depositing material onto a substrate to create the walls of a channel, or by selectively removing material from a substrate such that the trenches become the channels. These two methods can be described as additive and subtractive microfabrication, respectively[22]. A common example of each strategy can be seen in Figure 1.

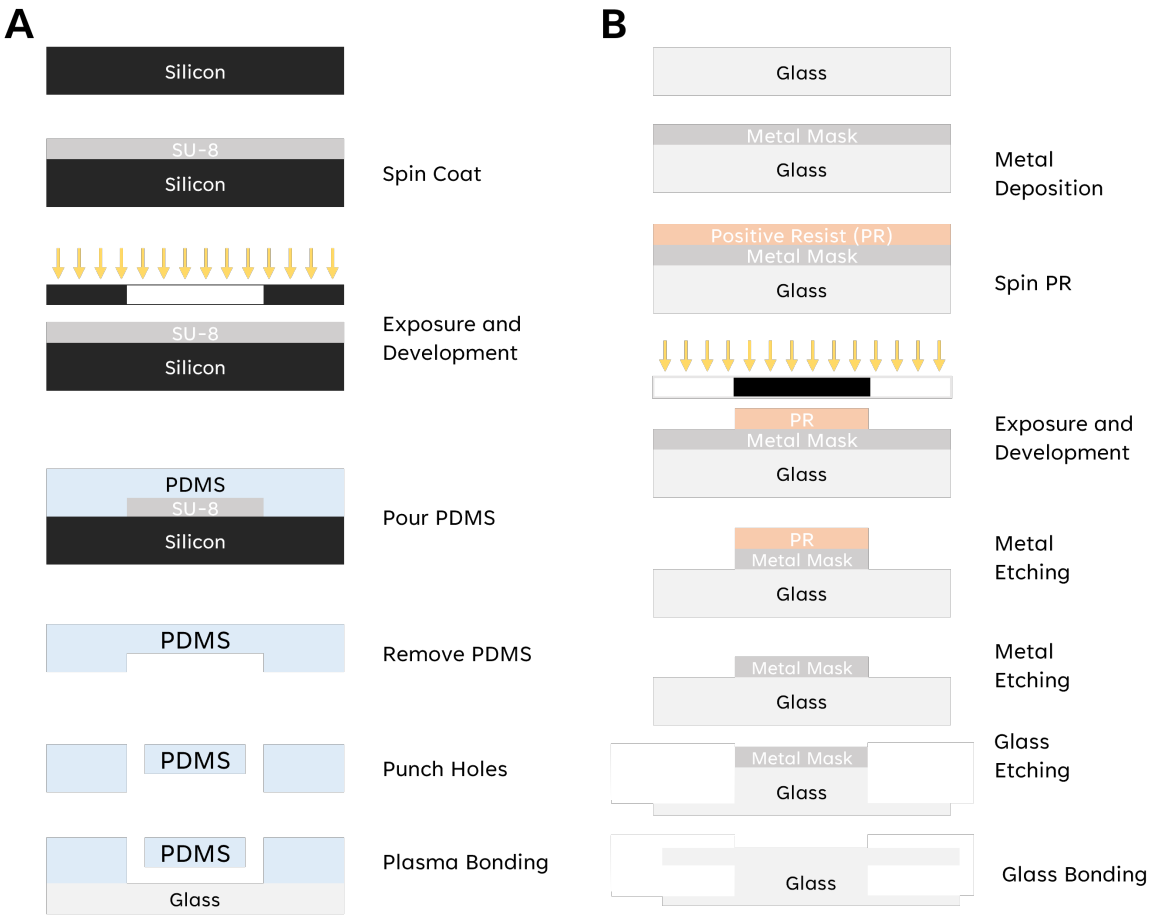

Figure 1: Example methods of both additive (A) and masking to prepare for subtractive (B) microfabrication.

2.2.1 Additive Microfabrication

Traditionally, to create microchannels by additive microfabrication, lithographic techniques are employed, including photolithography and soft lithography. Photolithography is the transfer of a

pattern to a photosensitive material by selective exposure to light[23]. A photosensitive material is a material that experiences a change in its physical properties when exposed to a radiation source[24]. If the material is selectively exposed to radiation, the pattern of the radiation on the material is transferred to the material exposed, as the properties of the exposed and unexposed regions differs. This facilitates selectively depositing material on a surface to form patterns.

These photosensitive materials are typically photoresists (also called resist, other photosensitive polymers are also used). These materials are deposited onto the surface of the substrate of choice (often a silicon wafer or glass slide), and spun very quickly to create a uniform thin film. Depending on the properties of the material, as well as the speed, acceleration, and duration of the spin, the height of this layer can be controlled[25].

After spin-coating a soft bake (also called a pre-exposure bake) is often performed. Here, the goal is to evaporate residual solvent that the photoresist polymer was dissolved in. This makes the resist more viscous, and results in decreases in layer thickness. This step avoids contamination from the mask getting into the resist layer, prevents the mask sticking to the resist, and improves the resist adhesion to the substrate[26].

To create a design or pattern in this resist layer, we selectively expose regions of the surface to radiation, often UV light. By using a photomask, we can block some of the exposure, functionally creating a shadow that transfers a projection of mask image into the resist, causing selective chemical property change. This changes the chemical resistance of the layer to a developer solution, which etches away either the exposed or unexposed regions. This difference depends on the formulation of the photoresist. If it is a positive resist, the exposed region is etched away by the solution, leaving behind the unexposed region. For the resist to be considered a negative resist, the exposed region becomes resilient to the developer solution, and the unexposed region gets solubilized[27] (Figure 2).

After exposure, a post-exposure bake is often performed to further decrease solvent content and help resolve the features by driving the reaction to completion[28]. A hard bake, which is another post-exposure bake, but generally at a higher temperature and for longer, is also done when using

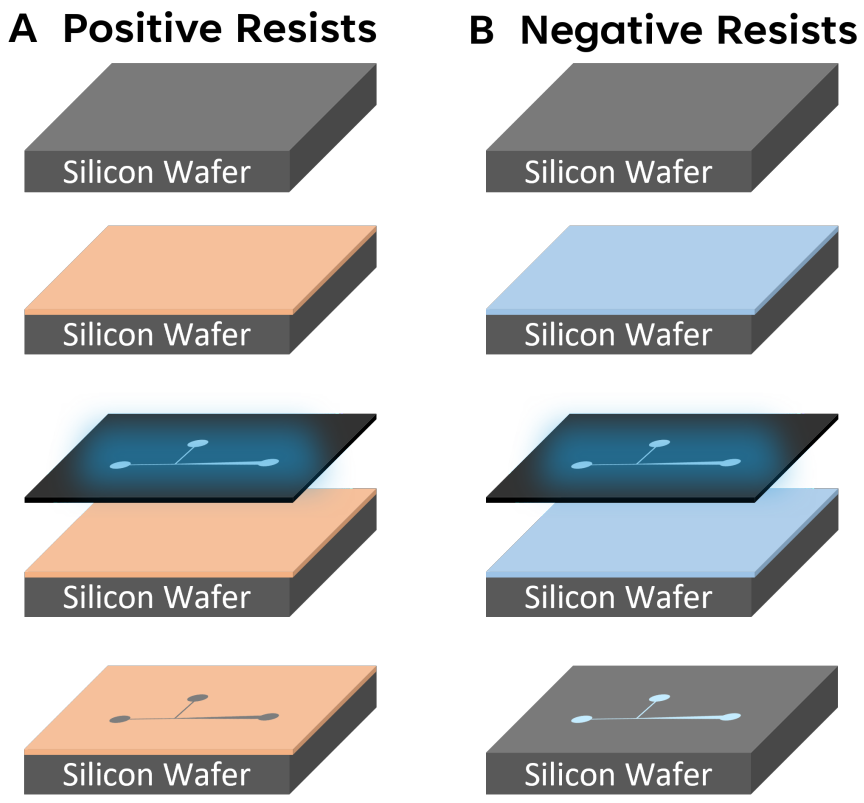

Figure 2: Positive (A) and negative (B) photoresists are exposed through a mask, and the resulting pattern difference as a result.

the resist as an etching mask to help make the resist more chemically or physically impervious to the etchant. Finally, the sample is placed in developer, often a tetramethylammonium hydroxide solution, to leave the final pattern.

At this point, the sample is a substrate, generally a silicon wafer or glass slide, with raised features. These features may be the walls of channels and all that is left is to seal off these channels. However this is not common, as the materials used for photolithography are not necessarily the most biocompatible or robust for these applications[29]. These features can act as sacrificial layers for a later step or act as a mask for an etching step, however, they are most commonly used to create 3D relief images in the shape of the desired channels. This is functionally a mold used to make the devices, through a process called soft lithography, often using a polymer called poly(dimethylsiloxane), or PDMS[30]. PDMS is biocompatible, permeable

to oxygen gas, elastomeric, and optically transparent, which makes it quite robust and compatible with many imaging modalities[31]. Another benefit of PDMS is the ability to easily form a covalent bond with glass using a plasma activation treatment, causing silanol groups (–OH) at the expense of methyl groups (-CH_3) on the surface[32]. When activated PDMS and glass slides are placed in contact, a siloxane bond (Si-O-Si) forms between them, creating a high-quality seal, and a completed traditional microfluidic device.

However, for the purposes of this thesis, it is important to note that this material swells in the presence of organic solvents[12], making it incompatible as the substrate containing the channels. There are other materials that are solvent resistant and able to be microfabricated, but given this resistivity, more complex microfabrication techniques, including the ones covered, and subtractive microfabrication, are necessary.

2.2.2 Subtractive Microfabrication:

For applications that use aggressive chemicals (organic solvents) and high temperatures, microchannels must be created in more versatile materials, e.g. glass and silicon. The most common techniques used for subtractive microfabrication, notably on glass and silicon substrates, are wet and dry etching processes. Wet etching uses liquid chemicals called etchants, where dry, or deep reactive-ion etching (DRIE), uses chemically reactive plasma, to selectively remove the material[33]. Generally, this selection is done by protecting certain parts of the sample from the etching mechanism with a mask which has been patterned with a design. Masks can be deposited onto the substrate via the previously discussed photolithographic steps, however, more robust masks can be made for aggressive wet etchants by including physical vapor deposition of metal.

The mechanism by which wet etching is accomplished is quite straightforward. The partially protected substrate is immersed in the solution, which then chemically etches the surface of the exposed substrate[34]. In most cases, hydrofluoric acid (HF) is used as the main etchant for any type of silicate materials[34]. The chemical reaction for etching is glass and silicon wafers is shown below:

$$SiO_2 + 6HF \longrightarrow H_2SiF_6 + 2H_20$$

Some other components, such as HCl, HNO_3, and NH_4F-buffer may also be added to control the etch rate[34]. Mask selectivity is generally well established, using metals like titanium, chromium, and gold to protect the surface. However, wet chemical etching is isotropic, meaning the etching rate is constant in all directions. This causes etching under the mask and produces rounded side wall microchannels[35].

The mechanism by which dry etching occurs is through etchant gases or plasmas removing substrate materials through bombardment of ions[25]. This can be sub-divided into physical dry etching, chemical dry etching, and physical–chemical etching. For glass, a physical–chemical etching called reactive ion etching (RIE) is used. Specifically, for microfludic channels and their high-aspect-ratio structures, the process is known as deep RIE (DRIE)[25]. The etch cycle consists of two steps: etching and deposition. In the etching step, silicon is removed by SF_6. In the deposition step, supply gas is switched to C_4F_8[25]. A film of fluorocarbon polymer is deposited on the side walls and bottom. Then, the polymer film at the bottom surface is removed by ion bombardment, while the film at sidewalls is intact and protects the sidewalls from etching[25]. This process is more controlled and has been shown to be more anisotropic, however, achieving good selectivity is usually more challenging[25]. Additionally, in glass achieving smooth surfaces has been shown to be difficult[36].

Chapter 3

Design and fabrication of a solvent compatible, high fidelity, droplet microfluidic device.

3.1 Introduction

Here, we optimized a protocol for accomplishing high-fidelity glass microchannel fabrication, summarized in Figure 3. The overall strategy is to pattern on a negative resist in the shape of the desired channels as a sacrificial layer such that a hard metal mask is deposited on both the surface of the glass and the photoresist pattern. When the photoresist is removed with a simple solvent wash, the resulting sample is a glass slide with a metal mask protecting the surface except where the resist was, allowing for selective surface etching in the desired pattern.

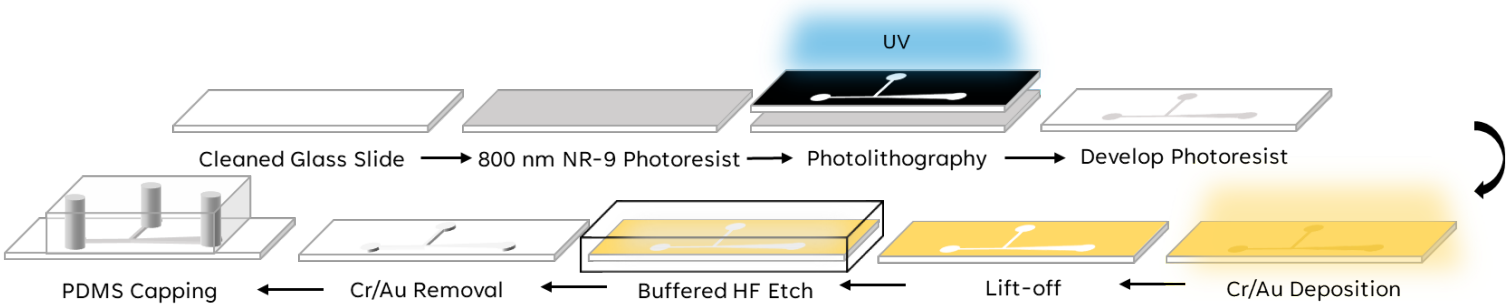

Figure 3: In-house recipe for microfabrication of a glass microfluidic device.

3.2 Materials and Methods

All microfabrication activities were performed in the Vanderbilt Institute of Nanoscale Science and Engineering (VINSE) class 100/1000 cleanroom.

3.2.1 Photomask Design

Computer-aided design (CAD) software, AutoCAD 2022 Student (Autodesk, Inc.), was used to draw the initial design for the photomask. Channel dimensions were drawn to be 50 µm, and inlet holes were drawn to be 2 mm. Using this CAD file, a negative photomask was made by VINSE staff in chrome and glass.

3.2.2 Substrate Preparation

The substrate chosen for fabricating glass microfluidic devices were precleaned, Starfrost borosilicate glass slides (Electron Microscopy Sciences). To degrease and remove dust from the surfaces, slides were first sonicated in an acetone bath, rinsed with more acetone, followed by isopropyl alcohol (IPA), and finally blown dry with a nitrogen gas gun. To further clean the surfaces, slides were oxygen plasma treated in a Trion Phantom II. Soda-lime glass microscope slides were also used before they were determined to be less effective due to some inherent surface roughness and defects. These were Fisherbrand Premium pre-cleaned plain glass microscope slides (Fisher Scientific.)

3.2.3 Photolithography

Cleaned glass slides were immediately taken to a separate bay the cleanroom which blocks UV light to begin photolithography. Slides were placed into a spin coater, centered on a 3/4 inch vacuum area spinchuck (Cost Effective Equipment) such that the vacuum area was smaller than the width of the slide. Using a plastic pipette, the slide was covered with a small amount of NR9-1000PY (Futurrex, Inc.) and spun using an experimentally determined spin recipe at 5000 RPM for 40s to achieve a layer height of 800 nm. Samples were then baked for a pre-exposure bake for 60 seconds at 150°C and then allowed to cool. Then, the samples were exposed to 400 mJ of UV light through a chrome negative photomask (made by VINSE staff) on a Karl Suss MA-6 mask aligner. Exposure time was calculated before every exposure by measuring the power of the lamp at the 365 nm wavelength with a UV optometer (Gigahertz-Optik GmbH) and using the following equation:

$$Exposure\ Time\ (s) = \frac{Exposure\ Dose\ (mJ/cm^2)}{Lamp\ Power\ (mW/cm^2)}$$

After exposure, another bake was performed at 100°C for 60 seconds, and allowed to cool. Unexposed photoresist was removed by agitating the sample in a bath of Microposit MF-319 developer (Shipley Company) for 30 seconds, washing with DI water, and drying with a nitrogen

gun. All samples were observed under an optical microscope to check for defects before moving to the next step. If a defect was found, the photoresist was removed with acetone and IPA and the process was run again beginning with the spin coating step.

Other photoresists were used during attempts at wet etching through a polymeric mask, including S1813 and S1818 (Shipley Company), as well as SPR 220 4.5 and SPR 220 7.0 (Rohm and Haas Electronic Materials). As part of this, an adhesion promotion step was performed by treating the surfaces of the glass slides with hexamethyldisilizane (HMDS) in a 310TA HMDS Vapor-Prime and Image-Reversal Vacuum Oven (Yield Engineering Systems).

3.2.4 Hard Masking

Defect-free patterned samples were coated with a 50 nm layer of chrome (Cr) and a 400 nm of gold (Au) using a multimode physical vapor deposition chamber (Angstrom Engineering). Chrome was deposited via resistive thermal evaporation at a deposition rate of 0.4 A/s. Gold was deposited via electron-beam evaporation at a deposition rate of 0.8 A/s. To avoid the samples from getting too hot, gold deposition was performed in two bouts of 200 nm, with a full venting and pump down of the chamber in between.

After metal deposition, the sacrificial layer of photoresist was removed with an acetone wash, along with the metal that was deposited on top, revealing a metal protective layer covering the surface of the glass except in the shape of the pattern (see Figure 6). To ensure successful lift-off, all the steps up to this point were done sequentially. Waiting too much time between photolithogrpahy and deposition/lift-off or waiting too long to do lift-off can result in redeposition of the metal on the sacrificial layer onto the glass surface.

3.2.5 Wet Etching

To etch microchannels into the surface of the glass, samples with a metal mask were placed into various hydrofluoric acid (HF) solutions. Etching was attempted in 50% HF (Sigma-Aldrich), as well as a solution of 5% buffered HF solution (Transene Company, Inc.) and 9.25% hydrochloric acid (HCl) to help remove insoluble products of silicon dioxide etching. Depth is controlled by the

etch time. Etching for 210 minutes at 42°C with stirring at 120 RPM achieved the target channel depth of 50 μm. Gold and chrome layers were removed with respective etch solutions (Transene Company, Inc.)

3.3 Results

3.3.1 High Resolution Patterning of a Sacrificial Photoresist Lift-off Layer

Successful patterning of an 800 nm NR9 resist can be observed in Figures 4 and 5. The pattern on the sample is defect free, well resolved with vertical walls, and feature sizes match that of the original design on the photomask. This suggests an optimized recipe with the correct exposure dose and bake times for the desired thickness and aspect ratio.

Figure 4: Brightfield imaging of a well-resolved NR9 pattern at junction.

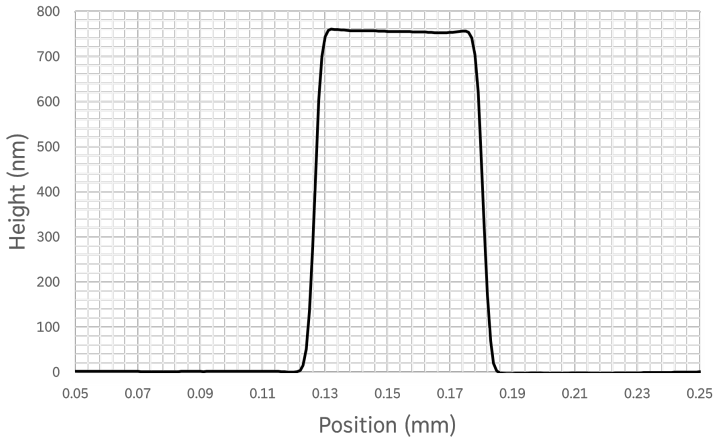

Figure 5: Surface profile of the sacrificial NR-9 life off layer as measured by profilometry.

Successful metal deposition and the removal of the sacrificial photoresist layer can be seen in Figure 6. At this point, the surface of the glass is only exposed in the shape of the pattern to be etched (i.e. the entire surface is protected except where the photoresist was.) The edges are well

defined and there are no visible defects along the wall or in the masking layer itself, suggesting an effecting masking against the etchant.

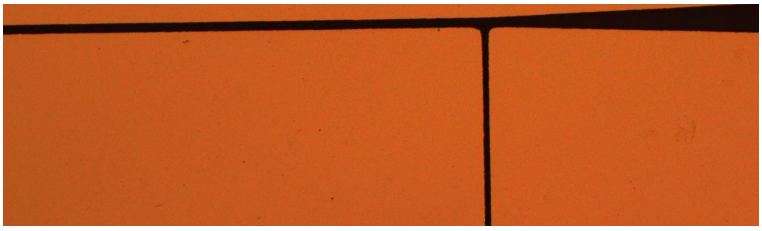

Figure 6: Surface of the glass after lift-off of the photoresist.

3.3.2 Optimization of Masking and Etching to Reduce Off-target Etching, Defects, and Surface Morphology

Significant optimization was necessary to produce high quality glass microchannels. The first attempt at glass etching was through a polymeric mask, using positive photoresists. Troubleshooting for this included attempting multiple photoresist formulations, thicker spin coats, improving layer adhesion with a hexamethyldisilizane (HMDS) treatment and performing a hard bake step. All of these proved to be unsuccessful because the desired depth of 50 μm required a relatively long etching incubation, which these materials were unable to withstand. This lead to the decision to move forward with using a negative resist as a lift off layer for metal masking, which demonstrated significantly better resilience to etching solutions (Figure 7.)

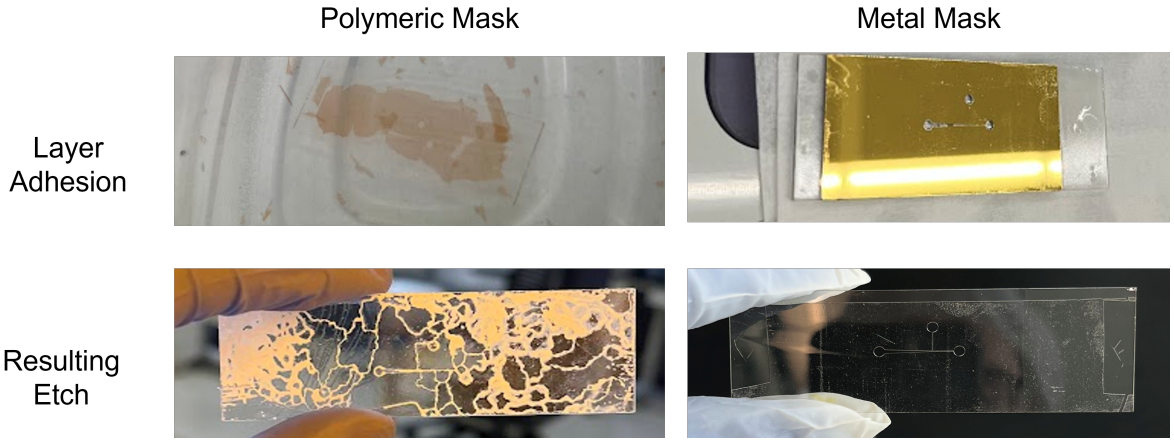

Figure 7: Resilience of a polymeric mask versus a metal mask to hydrofluoric acid etching.

By iterating over certain aspects of the recipe, we were able to reduce off-target etching, wall defects, and avoid insoluble products from depositing into the channels. Increasing the thickness of the hard mask reduced off-target etching (Figure 8 A, B). The first attempt at metal masking employed a 30 nm chrome adhesion layer and a 100 nm gold protective layer (30/100 Cr/Au.) This proved to be more efficacious than the polymeric masks, but still resulted in flaking off of the mask during etching, leading to very large defects that often rendered the devices useless. This is evident in Figure 8 A, where the two inlet channels are connected by a large defect, which would cause fluids to mix in unpredictable ways and affect the flow profile.

To improve the mask's resilience, we increased the chrome layer to 50 nm and the gold layer to 400 nm, which was the highest utilized in the literature[37]. Improving mask resilience decreased the amount of wall and surface defects, and the resulting channel width more closely matched the original design, but there were still defects in the channels that would affect the flow profile or the junction. Defects were further minimized by moving to borosilicate glass instead of soda-lime (Figure 8 C). This switch also improved the aspect ratio of the channels, or the channel width compared to the depth (Figure 9). In other words, we were able to etch deep channels while maintaing the 50 μm width.

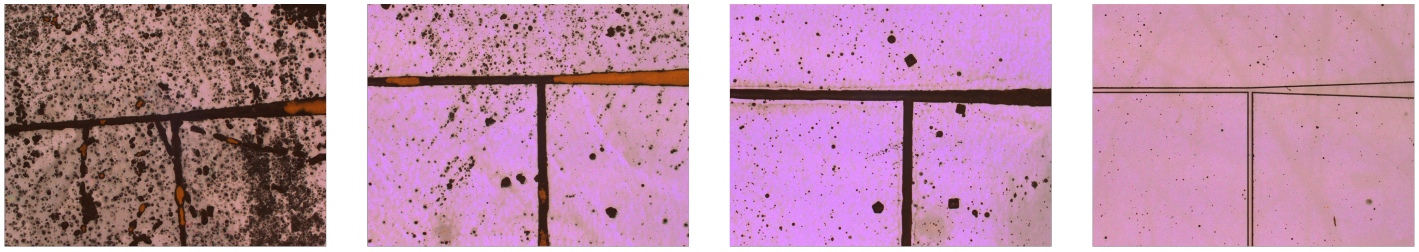

Figure 8: Metal mask iterations to improve off-target etching and channel defects. Insoluble products are the orange deposits in the channels in A and B.

Moving to a buffered HF solution further reduced defects in the channels (Figure 8 D) and decreased surface roughness. This can be seen visually in Figure 8 by comparing C and D, where

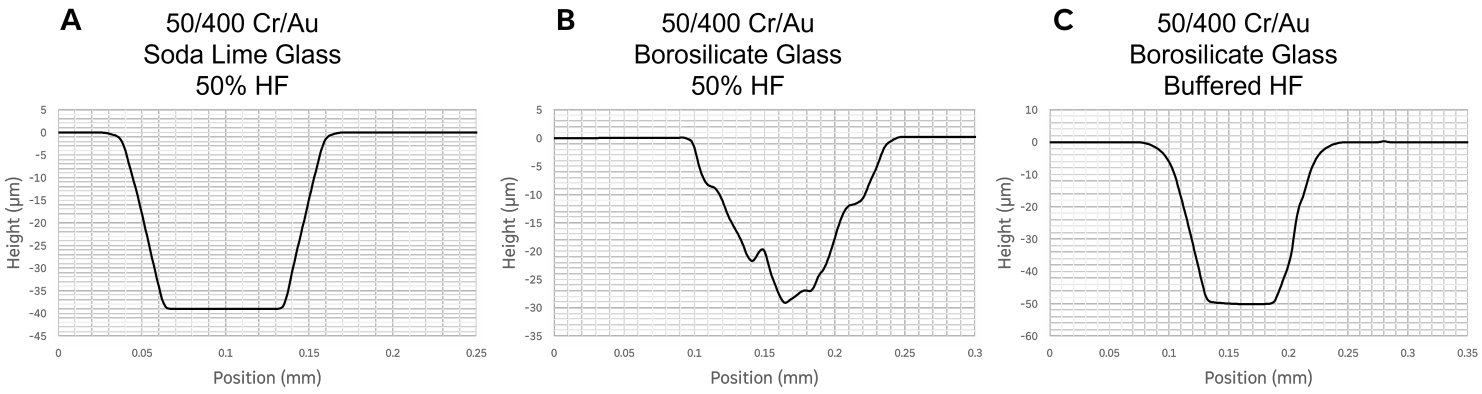

Figure 9: Improvements in channel profile and aspect ratio as measured by profilometry.

there are less pinholes on the surface, and the channels are now optically transparent, suggesting significant improvements in roughness. Surface roughness was quantified using a profilometer and demonstrated in Figure 10. The 50% HF etched device has a surface roughness range of about 30 µm, while the buffered HF etching channels has a range of about 20 nm, demonstrating improvements in surface roughness by three orders of magnitude. This will improve the consistency between devices, ensure laminar flow, promote droplet formation only at the junction, and prevent droplet breakup as they exit the device.

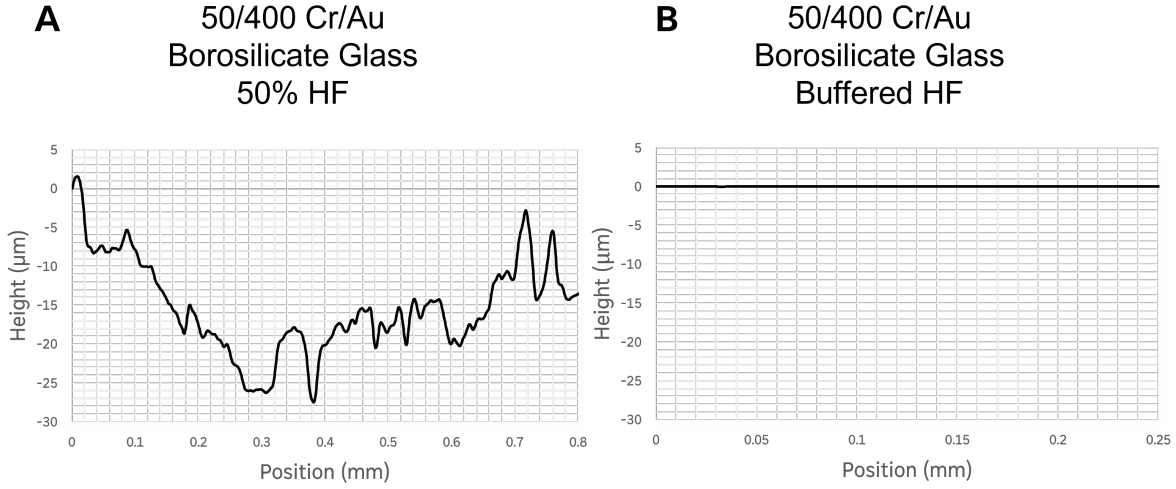

Figure 10: Improvements in surface roughness due to a buffered HF system as measured by profilometry.

3.4 Discussion

Glass microfluidic devices are necessary when traditional PDMS devices are incompatible with the desired solvents, as as is the case for the novel polymers being developed in our laboratory. Deep, high fidelity glass wet etching of borosilicate for microfluidics is difficult to achieve[38], and generally requires a combination of multiple complicated masking and sacrificial layers that necessitate an alignment step[37,39]. There is a demonstrated need to simplify this process for in-house development of glass microfluidic chips. Presented here is a simple method of glass microfabrication that yields microfluidic devices with high aspect ratios, low defects, and smooth channels. The methods can be seen in more detail in Section 3.2 and summarized is in Figure 3.

The general metric for success here was minimizing presence and severity of defects, generally called pinholes. Pinhole defects are a common problem in these types of masks caused by HF diffusion through the Cr/Au film and by defects on the Cr/Au film itself[37]. The pinholes become larger and in greater number the longer the etching time, thus limiting the etch depth to a point where the number of pinholes generated are unacceptable for further processing of the glass[40]. Here, the goal was to reach a channel depth of 50 μm, so minimizing pinholes while still reaching this depth was necessary. Avoiding pinholes is not only important for ensuring the pattern in that of the original design, but also that sealing off the channels is successful. PDMS has a lower quality bond, and can thus fail at necessary working pressures, if the surface of the glass is rough[41]. Roughness and defects also offer more avenues for fluid to flow into defects that are not the channels, which can cause loss of reagents, turbulent flow, and pressure buildup.

This method uses high quality borosilicate glass slides to avoid defects. Borosilicate glass tends to be cleaner and flatter with less defects[38], and because of these reasons, was a better surface on which to deposit a metal mask onto. Particulates that couldn't be removed and defects on the surface of soda-lime glass slides translated to defects in the mask, and thus etching defects. However, borosilicate is more difficult to etch, with a slower etch rate and more insoluble products[34], which led to better aspect ratios but rougher surfaces.

Devices etched in 50% HF had insoluble products deposited on the surface (which can be seen as orange coloration in the channels in Figure 8 B) which blocked etching, leading to inconsistent channel depths and thus high ranges of roughness. This was overcome by slowing the etch rate and doping in acids with a dilute buffered HF solution[42]. The buffering agents were ammonium and HCl, which help solubilize the insoluble products of silicon dioxide etching and ensured that the devices produced are consistent among batches.

Channel surface roughness is an important factor to consider in microfluidics. More generally, large depth ranges are to be avoided simply because the depth is not what is being targeted across the entire channel. This could promote alternative droplet formation modalities in different devices, leading to changes in resulting particle size, defeating the purpose of using microfluidics to improve monodispersity. Additionally, one of the main benefits of microfluidics is laminar flow, and if surface roughness is too high, this can become turbulent[43], leading to unwanted diffusion, or in the case of droplet microfluidics, droplet breakup or no droplet formation whatsoever. Laminar flow can also be disrupted by inconsistent channel widths from surface defects.

Another reason to avoid surface roughness specifically for this application is the affect roughness has on hydrophilicity of the channels. The topological nature of surface roughness has a major influence on the water repellency of surfaces[44], and to get droplet formation of the oil phase, the aqueous phase needs to have a high affinity for the walls, so it is necessary to keep the channels as hydrophilic as possible.

NR9-1000PY was chosen as the resist to use for the lift-off layer as it a negative resist, which can obtain a retrograde profile. This is much better for liftoff than positive resists, which give a straight or slightly graded profile. This is problematic because it can lead to "bridging" of the two metal layers. NR9 is specifically designed for lift-off in this way, as well as having good adhesion to the substrate and being easily strippable. The 1000PY formulation of NR9 is designed to be spun in the thickness range of 0.7 μm to 2.1 μm, which is a good range for ensuring there is a large enough distance between the two layer heights. The general rule for lift-off is to have the

resist layer height about twice the height of the deposition layer. In this case, the deposition layer was 450 nm and the lift-off layer was 800, which is approximately in that range and resulted in a clean liftoff. However, issues with liftoff did arise if photolithography and metal deposition did not happen in the same day. This is potentially due to the resist losing its strippability over long periods after exposure, as exposure initiates a polymerization/crosslinking of the NR9 monomers. The opposite could also be the case, i.e. the photoresist loses its crosslinking, which causes the metal to redeposit directly onto the surface of the glass. This has not been investigated, but running the finalized recipe within approximately an 8 hour period has never resulted in the same lift-off issues.

Letting the samples cool after the two bake steps during photolithography was important for improving consistency and success rate. Cooling after the pre-exposure bake made sure the initiation and propagation of the crosslinking process always happened at the same temperature, and thus rate. Cooling after post-exposure bake (before development) ensures the etching of the unexposed photoresist happened at the same temperature, as an elevated temperature may increase the etch rate and the solubility of exposed resist.

The choice of gold as a metal for the hard mask is well established in the literature[45], however the adhesion layer metal varies among the literature, generally between chromium (Cr) and titanium. Cr was chosen as it is more established in VINSE protocols, has a higher deposition rate, and is less precious. In general, the adhesion layer acts as a wetting layer for gold, reducing the energy barrier for bonding and increasing the number of nucleation sites compared to Au directly evaporated onto the SiO2 surface[46]. The enhanced wetting is due to the formation of an alloy with the adhesion layer, as well as the adhesion layer's higher affinity for oxygen in the glass compared to that of Au. Although both metals do not necessarily react with HF, the acid can diffuse through each metal individually; it is the formation of the alloy that blocks this.

A thicker metal layer was less likely to have defects, and was better able to block the diffusion of HF through the mask, leading to dramatically less defective surfaces. The buffered HF system also helped in this way, as the slower etch rate was less harsh on the mask. The etch rates were

quite different: 30 μm/min^{-1} in 50% HF and 0.24 μm/min^{-1} in buffered HF, even with heating and agitation. This was done to attempt to slightly improve the etch times to a more reasonable range. Without heating and agitation, the etch rate was 0.2 μm/min^{-1}. A less aggressive etchant also decreased the amount of underetching, which explains the improvements in aspect ratios. Channel widths are much closer to 50 μm in the buffered system.

A 400 nm gold layer is on the upper end of the literature in terms of achieving high fidelity[37,47], low defect glass etching. Although much of the gold is recovered from the gold etch solution, this still means the process developed may be more resource intensive in terms of raw material. However, this method offers benefits to those that use less gold in that it avoids the need for another photoresist layer. Many other methods use an AZ positive photoresist as part of the masking layer to protect the glass surface (e.g. Figure 1 B). These protocols can require multiple exposures, an alignment step which can be difficult, and more lift-off/development steps, including a selective metal etch before the HF etch that can often introduce defects into the masking layer, and thus the surface[37].

3.5 Conclusion

Glass as a substrate is a robust material for microfluidics, but etching to a depth of 50 μm for the purposes of producing large polymeric microparticles is difficult to do consistently and effectively. By combining a simple negative resist lift-off layer, thick gold hard masking with a Cr adhesion layer, and a buffered HF etching system, we developed an in-house, simple, alignment-free, resist-free hard masking protocol to microfabricate high-quality, glass microfluidic devices. Off-target etching and channel wall defects were minimized, and surface roughness was improved by three orders of magnitude, while reaching the target depth and aspect ratio. While these devices are high quality in their surface metrics and fidelity to the original design, testing is required to determine if the device successfully generates, and improves upon quality metrics for, polymeric microparticles.

Chapter 4

Demonstrating improvements in monodispersity of microfluidic generated polymeric microparticles over benchtop emulsions.

4.1 Introduction

Microparticle formulations can improve clinical outcomes[1], but the bulk emulsion method of producing these can lead to poor quality metrics. To resolve this, we will use the microfabricated chips from Chapter 3 to generate polymeric microparticles, and observe differences in quality metrics as compared to the bulk emulsion formulation (Figure 11. Bonding methods for sealing the microchannels were evaluated by checking for the presence of fluid outside of the channels. Thermal and adhesive bonding methods proved to be unsuccessful, however, PDMS capping sealed the channels well and was relatively solvent resistant. These devices, when two immiscible phases were introduced, promoted droplet formation of the water phase. However, given the goal of making polymeric microparticles loaded in the oil phase, the reverse emulsion was necessary. This was accomplished by modifying the surface of the channels to be more hydrophilic, ultimately with a novel polymeric zwitterionic silane, such that the water phase had a higher affinity for the walls of the channels and became the continuous phase. PLGA microparticles were successfully generated using the device and demonstrated preliminary improvements in quality metrics, notably the polydispersity index (PDI). Additionally, a crystalline polysulfide microparticle formulation was generated microfluidically, and demonstrated good quality metrics.

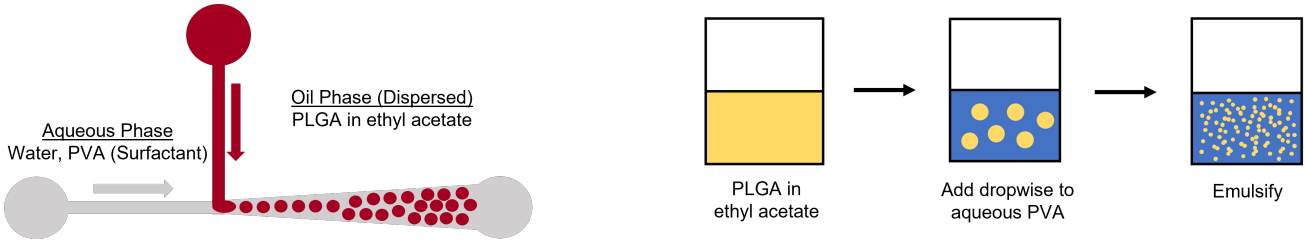

Figure 11: The two methods being compared against to determine if microfluidic-assisted fabrication (left) improves monodispersity of resulting particles compared to the benchtop bulk emulsion (right)

4.2 Materials and Methods

4.2.1 Surface Activation

To activate surfaces for PDMS bonding and surface treatments, samples were exposed to a 2 minute atmospheric air plasma treatment on the "high" power setting in a plasma cleaner (PDC-001, Harrick Plasma). The vacuum was allowed to build up pressure in the chamber for 1 minute prior to turning on the RF switch. Because only the surfaces in contact with the air become activated, samples were placed in with the bonding side up.

4.2.2 PDMS Capping

Polydimethylsiloxane (PDMS) (SYLGARD™ 184, Dow Corning) was prepared by mixing a 10:1 ratio of base to curing agent. This was mixed vigorously for 5 minutes, poured into a petri dish, degassed in a desiccator for 30 minutes (or until bubbles are gone), and baked for 2 hours at 65°C. Pieces of PDMS were cut to be large enough to cover the channel pattern, and inlet holes were created using a 1.5mm biopsy punch, poking holes by eye over a stencil pattern. Since inlet holes in the pattern are larger than the punch, there is some room for error here.

To seal the channels, the glass slide and a piece of PDMS were plasma activated with the bonding side up, aligned by eye, and placed in contact. Both parts were cleaned before treatment. The glass slides were solvent cleaned and nitrogen blow dried. For PDMS, dust was removed with PVC surface protection low adhesion cleanroom tape (Ultratape).

4.2.3 Synthesis of APTES-Zwitter

In a PTFE reaction flask, 4.0 g of [2-(methacryloyloxy)ethyl]dimethyl-(3-sulfopropyl ammonium hydroxide) (DMAPS) were added to 4 mL of trifluoroethanol (TFE) with 334 mg of (3-Aminopropyl)triethoxysilane-4-cyano-4-(ethylsulfanylthiocarbonyl) sulfanylvpentanoic acid (APTES-ECT) and 46.3 mg of VA-044 (Wako Chemicals) (Figure 12). The resulting solution was purged with nitrogen gas for 20 minutes, heated to 55°C, and allowed to react overnight. The mixture was precipitated into an excess of diethyl ether. The first precipitate was redissolved in

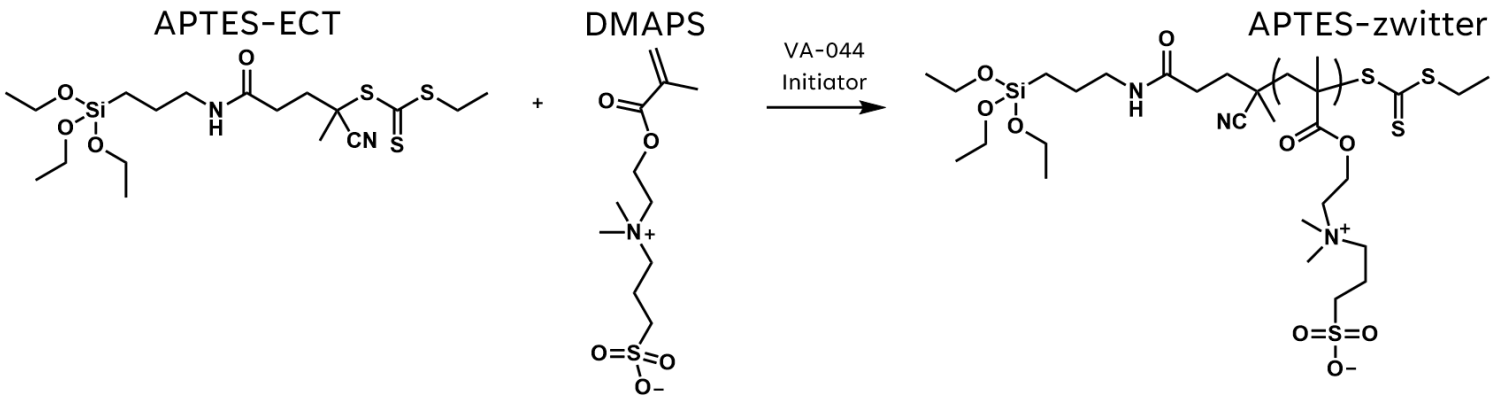

Figure 12: Polymerization reaction schematic of the APTES-zwitter surface coating

acetone and precipitated three times. The final solid, the APTES-zwitter, was dried in the vacuum oven over 2 days to give the final product.

4.2.4 Surface Treatments

A silane-PEG treatment solution was prepared by dissolving 5K silane-PEG (Creative PEGWorks) at 1mg/mL in DMSO. Surfaces functionalized with this solution were prepared by plasma treating an already sealed device, flowing the solution into the channels, and letting incubate for 2 hours. The solution was then washed away with DMSO.

(3-Aminopropyl)triethoxysilane (APTES) (Sigma Aldrich) functionalized devices were prepared by plasma treating an already sealed device, flowing a 5% APTES in ethanol solution into the channels, and immediately washing with more ethanol.

An APTES-zwitter treatment solution was prepared by dissolving the final product of the synthesis reaction described above at 100 mg/mL in a co-solvent of 30% DMSO and 70% PBS. Surfaces functionalized with this solution were prepared by flowing the solution into the channels immediately after plasma bonding and letting them incubate for at least 30 minutes. After incubation, the treatment was removed by blowing nitrogen gas into the channels, and washing with more DMSO/PBS.

Devices were also made to have PVA adsorbed to the surface by flowing in 1.5%PVA into plasma treated channels, letting incubate for 10 minutes, blowing nitrogen gas into the channels,

and baking at 110°C for 15 minutes. This was repeated two more times, without a plasma treatment.

4.2.5 Microfluidic Setup

Microfluidic adaptors and components here were purchased from Dolomite Microfluidics unless otherwise specified. Fluids were introduced into, and collected from, sealed devices via tubing inserted into the punched holes of the PDMS. 1.6 mm OD x 0.8 ID PTFE tubing was connected to 0.5 mL Gastight Syringes (Hamilton) using ETFE ferrules for 1.6mm OD tubing, Delrin end fittings with 1/4“-28” threads, and Tefzel 1/4“-28” female thread to female Luer lock. All wetted surfaced are organic solvent resistant. Syringes were immobilized in programmable flow rate syringe pumps (PicoPlus, Harvard Apparatus). Outlet tubing was placed directly into the hardening solution.

4.2.6 Microfluidic Formulation of PLGA Microparticles

The protocol for the etched glass slides used to generate PLGA microparticles is the final optimized recipe outlined in Chapter 3. Briefly, these are borosilicate glass sides etched in buffered HF through a 50/400 Cr/Au hard mask.

The oil phase for these batches consisted of 1% weight Resomer® RG 503 H PLGA (Sigma Aldrich) dissolved in ethyl acetate. The water phase consisted of 1.5% poly(vinyl alcohol). The flow rates of the oil and water phases were 200 $\mu L/hr^{-1}$ and 400 $\mu L/hr^{-1}$, respectively.

4.2.7 Bulk Emulsion (Benchtop) Formulation of PLGA Microparticles

1% weight Resomer® RG 503 H PLGA (Sigma Aldrich) dissolved in ethyl acetate was added slowly to a 1.5% PVA solution. This was emulsified by stirring at 1000 RPM for 60 seconds, and then poured into the hardening solution.

4.2.8 Microfluidic Formulation of Polysulfide Microparticles

The protocol for etched glass slides used for these polysulfide microparticles was in devices made similarly to the finalized version, but etched in 50% HF (see Figures 8C and 9B.)

The oil phase for these batches consisted of varying percent weight polysulfides dissolved in ethyl acetate, dichloromethane, chloroform, or some combination of the three. The water phase consisted of 1.5% PVA. The flow rates of the oil and water phases varied, but a flow rate ratio of 1:2, respectively, was maintained. The successful batch shown in Figure 21 was made with a 60% propylene sulfide 40% ethylene sulfide copolymer dissolved at 50 mg/mL in DCM. The flow rates of the oil and water phases were 400 $\mu L/hr^{-1}$ and 800 $\mu L/hr^{-1}$, respectively.

4.2.9 Particle Hardening and Processing

The hardening solution consisted of 0.1% PVA in DI water stirring at 250 RPM to avoid aggregation and promote hardening. Particles made by microfludics and on the benchtop were processed the same way, although microfluidically generated particles were added to the hardening solution as they left the device, whereas the benchtop formulation was added in bulk. Particles were allowed to harden for 10 minutes, which began at addition for the benchtop particles, but once the system was turned off for the microfluidic formulation.

After hardening, the particles were spun down at 300 RCF for 3 minutes, resuspended in 500 µL and aliquoted into preweighed tubes. These were then sonicated to ensure homogenous resuspension and avoid aggregation, then quickly flash frozen in liquid nitrogen and lyophilized overnight.

Lyophilized particles were resuspended at 20mg/mL in a suspension buffer of 25mg/mL Pluronic® F127 (Sigma Aldrich) and 25 mg/mL carboxymethyl cellulose. This was then washed off by centrifuging at 300 RCF for 3 minutes and resuspending again in DI water at 20 mg/mL.

4.2.10 Imaging and Analysis

Images of the particles were taken on a Zeiss Merlin Scanning Electron Microscope (SEM) with a Gemini II Column. Once particles were hardened, lyophilized, and then resuspended, 20 µL

of suspended particles were placed on a copper tape covered SEM stub and allowed to evaporate over at least few hours, leaving behind just particles. To prepare the samples for SEM imaging, the surface must be conductive. To accomplish this, stubs were taken to a gold sputter coater and treated for 20 seconds to deposit a thin, slightly purple appearing, layer of gold. These can then be transferred into the SEM for imaging. All images were taken at 2048 x 1536 resolution for quantification and collected using the secondary electron (SE2) detector.

SEM images were processed and quantified using an in-house developed MATLAB script. The script imports an SEM image from the local path and crops out the banner that is generated by the imaging software. This banner contains information about the conditions in which the image was taken on the SEM, including the scale bar size. The program does an edge detection pre-processing step using the `edge()` function, and then a Hough Line Transform to detect straight lines. This number is the length in pixels of the scale bar. To convert this into microns such that the size of the particles can be determined and compared across images, the `ocr()` function was employed to do optical character recognition on the region of interest to read the length in microns of the scale bar.

The `imfindcircles()` function was used to detect particles in the image and find their size in pixels. This function takes in a maximum and minimum radius, as well as a sensitivity factor, as inputs, and these were adjusted for every image to get the more accurate particle detection. The matrix of radii in pixels is then converted to microns using the scale bar, and the associated statistics, including polydispersity index (PDI), were calculated for the batch. PDI was calculated using the following formula, where PDI=the square of the sample standard deviation divided by the mean particle diameter. :

$$Polydispersity\ Index\ (PDI) = \left(\frac{\sqrt{\frac{1}{N-1}\sum_{i=1}^{N}(x_i - \overline{x})^2}}{d}\right)^2$$

The full commented code is included in the appendix.

Droplet formation visualization in the device was done with a digital handheld microscope (TAKMLY) connected to a PC using built-in image capture software.

4.3 Results

4.3.1 PDMS Bonding is Necessary for In-House Device Sealing

In order to move from an etched glass slide with microchannels on the surface to a functional microfluidic device, the microchannels need to be sealed. Since glass is the best option for solvent compatibility, the first attempt at sealing the devices was by bonding the etched slide to another glass slide with inlet holes drilled in.

The first method attempted for glass bonding was to spin coat a thin layer of polyimide onto the top glass and place the two in contact. This proved unsuccessful, even with adjustments to polyimide formulations, spin speeds, bake times and temperatures, and amount of pressure applied. The seal between the two slides was never robust enough to block the flow of fluid everywhere but the channels (Figure 13), and without clogging the channels themselves.

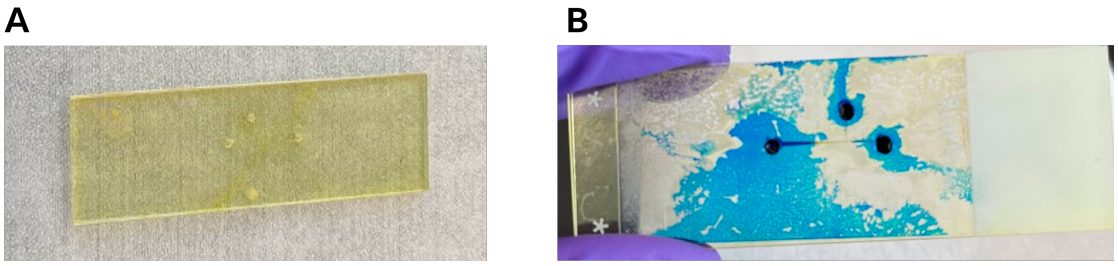

Figure 13: Polymeric bonding of glass slides. **(A)** Complete monolayer of polyimide between two glass slides **(B)** Incomplete sealing of spin coated polyimide bound devices.

The other method attempted was to thermally bond the slides in a tube furnace. This also proved unsuccessful, even with adjusting temperatures and ramp speeds, and priming the glass with plasma and acid treatments. Slides would either be completely unsealed, transiently bonded, or partially fused together and fragmented (Figure 14).

Once glass was ruled out as an option, a plasma treatment was done to both a piece of PDMS and the etched slide, and placed in contact. This, trivially, resulted in successful bond that could withstand all pressure ranges of experimentation (Figure 15).

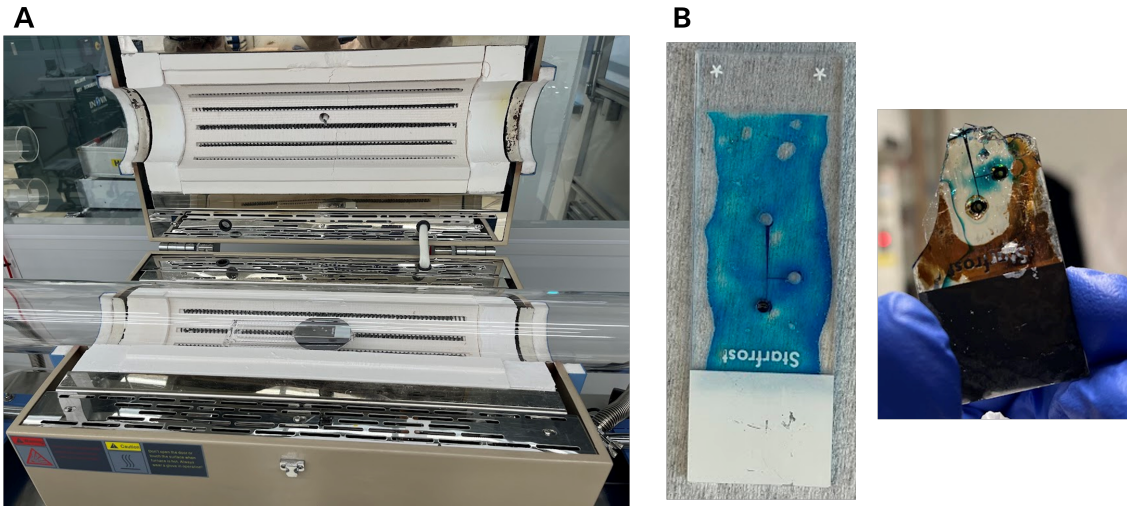

Figure 14: Thermal glass bonding. **(A)** Setup of the samples in a tube furnace **(B)** Incomplete sealing and fragmentation of thermally bound devices.

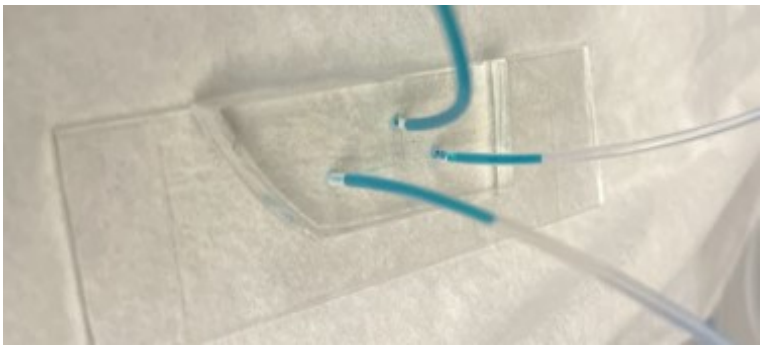

Figure 15: Sealed device with blue food dye flowing in the channels.

4.3.2 In-House Fabricated Glass Microfluidic Devices Promote Droplet Formation

In parallel with the iterations discusses in Chapter 3, initial prototypes of this T-junction droplet microfluidic device were taken out of the cleanroom to begin observing droplet formation.

In a 50% HF etched device, ethyl acetate was flown into the oil inlet, while water with blue food dye was flown into the water inlet. Interestingly, and opposite of what was desired, the device formed water-in-oil (W/O) droplets (Figure 16) as opposed to oil-in-water (O/W), even across a large range of flow rate ratios. This suggested that the surfaces of the device need to be more hydrophilic, leading to an effort to improve surface roughness (see Chapter 3), as well develop a protocol for hydrophilic surface treatments.

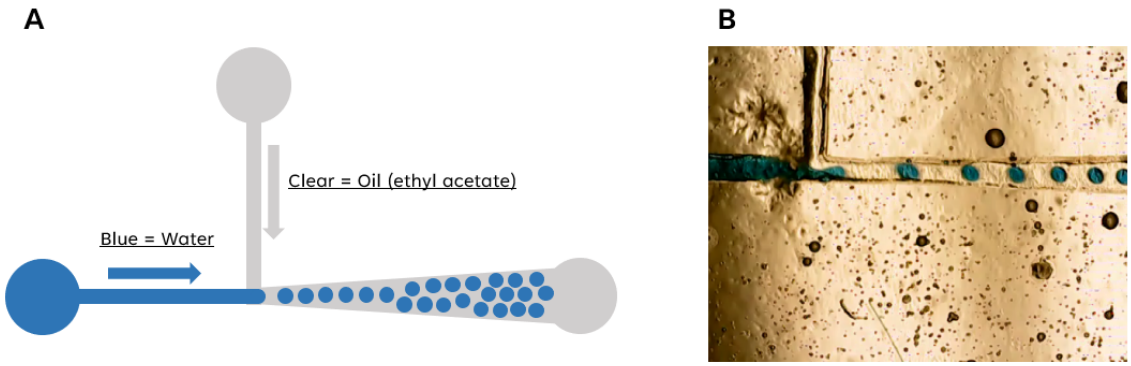

Figure 16: Water-in-oil droplet formation. **(A)** Visual schematic of the composition of each fluid phase. **(B)** Live droplet formation in the device.

4.3.3 Hydrophilic Surface Modifications Promote O/W Droplet Formation

Multiple surface treatments were tested to help improve hydrophilicity of the device walls, with the metric of success being that O/W droplets would preferentially form over W/O. The three surface treatments applied and their chemical structures can be seen in Figure 17 A, and the resulting droplet formation can be seen in B. The silane-PEG treatment did not promote droplet formation. This is demonstrated by a co-flow of both the oil phase and water phase after treatment. This means the oil phase had an affinity towards the walls of the channels, which is the phenomenon the surface treatment is supposed to avoid. APTES did promote droplet formation, however, this treatment had a tendency to clog the channels. Therefore a molecule of APTES was modified with a zwitterionic polymer to create a novel, ultrahydrophilic, surface coating that doesn't self condense. This also proved to be successful in promoting droplet formation (Figure 17).

4.3.4 Microfluidic Generation of PLGA Microparticles Improves Quality Metrics Over Bulk Emulsions

To test if there is an improvement in quality metrics when using microfluidics over the bulk emulsion, PLGA microparticles were made both via microfluidics and bulk emulsion. Both formulations were made twice, to test for consistency between batches of the same formulation. Using the flatter, buffered HF etched devices (Figure 8 D), with an ATPES-zwitter treatment, two

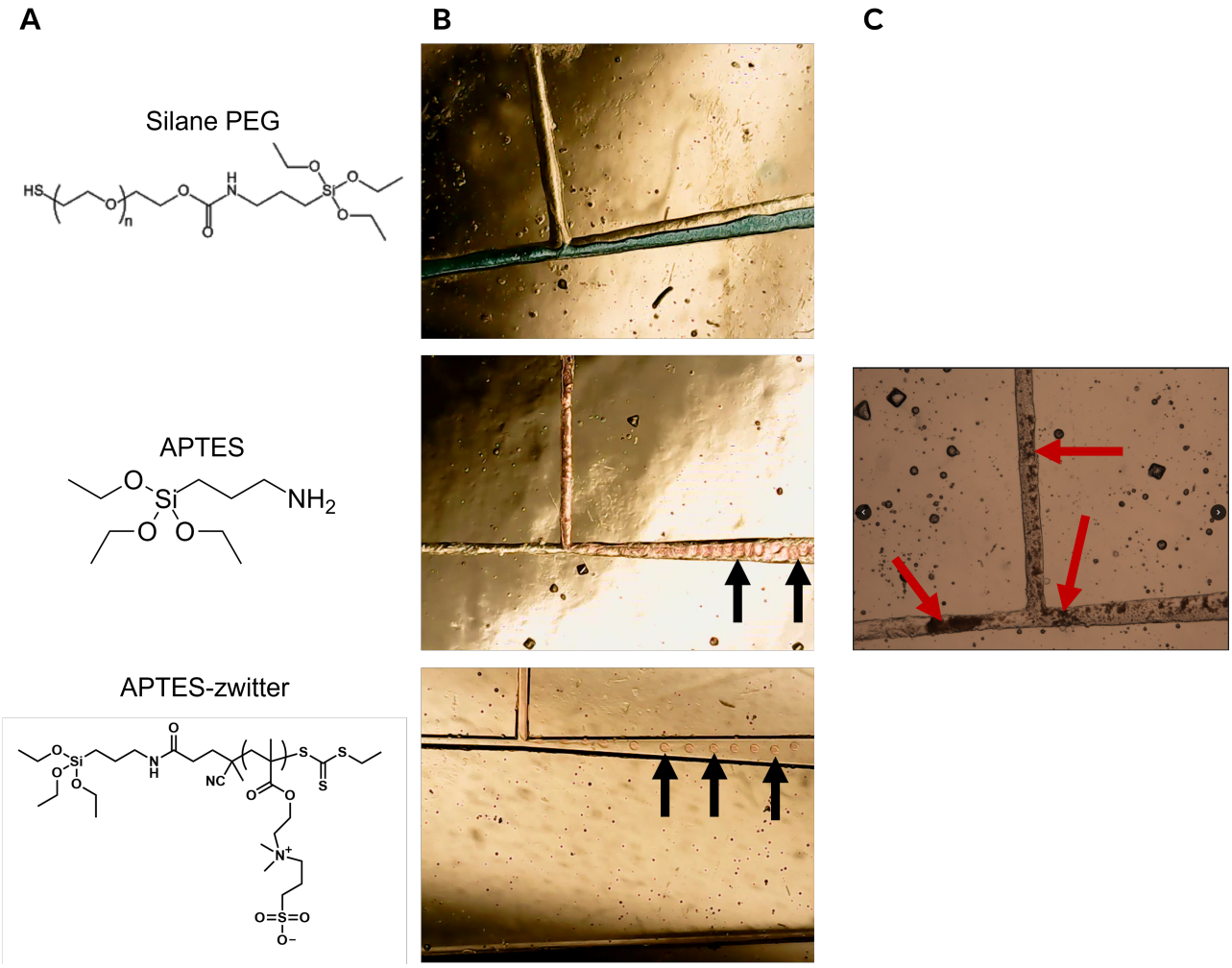

Figure 17: Surface modifications and their resulting effect on droplet formation. **(A)** The chemical structures of the applied surface treatments. **(B)** Flow profile of the resulting treatment in the device. Black arrows highlight droplets moving along the channel. **(C)** Aggregates of APTES clogging the channels after treatment. Red arrows point to large aggregates of APTES.

batches of PLGA microparticles were made and collected. These were compared against two batches of PLGA microparticles made via the bulk emulsion method. Images were processed using MATLAB, and the resulting circle detection and histograms with quality metrics can be seen in Figure 18. The resulting histograms of all four batches can be seen in Figure 19. The two microfluidic formulations had lower PDIs, smaller ranges, and were more consistent between batches than the benchtop formulation.

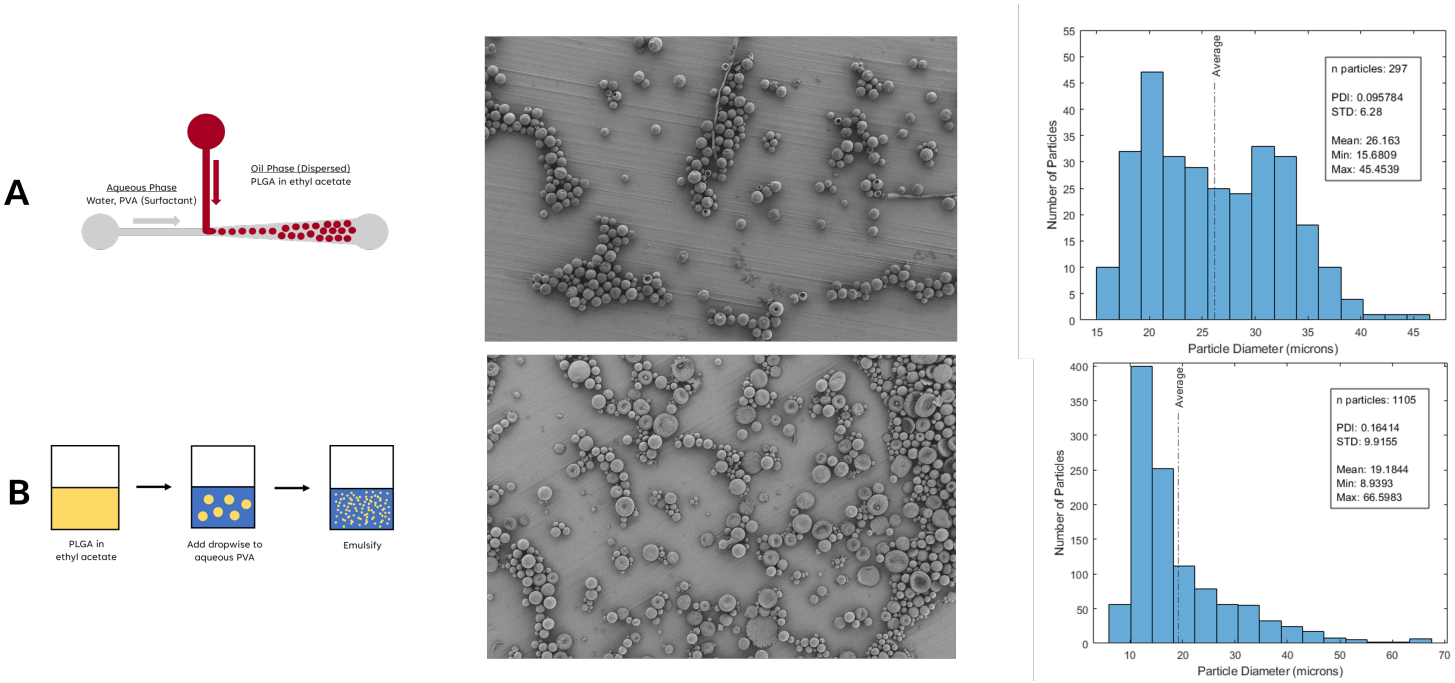

Figure 18: Generation method, SEM image of collected particles, and resulting data from each image for both the **(A)** microfluidic and **(B)** bulk emulsion formulations.

4.3.5 Preliminary Generation of Polysulfide Microparticles

As the ultimate goal of this device was to generate microparticles out of crystalline polymers which require organic solvents, droplet generation was attempted with a co-polymer of propylene sulfide (PS) and ethylene sulfide (ES) (PPSES) (Figure 20), which is only soluble in DCM or chloroform. Although many batches were attempted, both in earlier iterations of glass slides, and with various surface coatings, polymer concentrations, and solvents, it as difficult to produce these particles in this system consistently. However, successful batches have been made using a polymer of 60% PS to 40% ES dissolved in DCM with an APTES surface coating in a 50% HF etched device (seen in Figure 17). The resulting particles were highly monodisperse, as shown in Figure 21. This preliminary data suggests this system, with additional optimization, will be consistently successful at producing MPs.

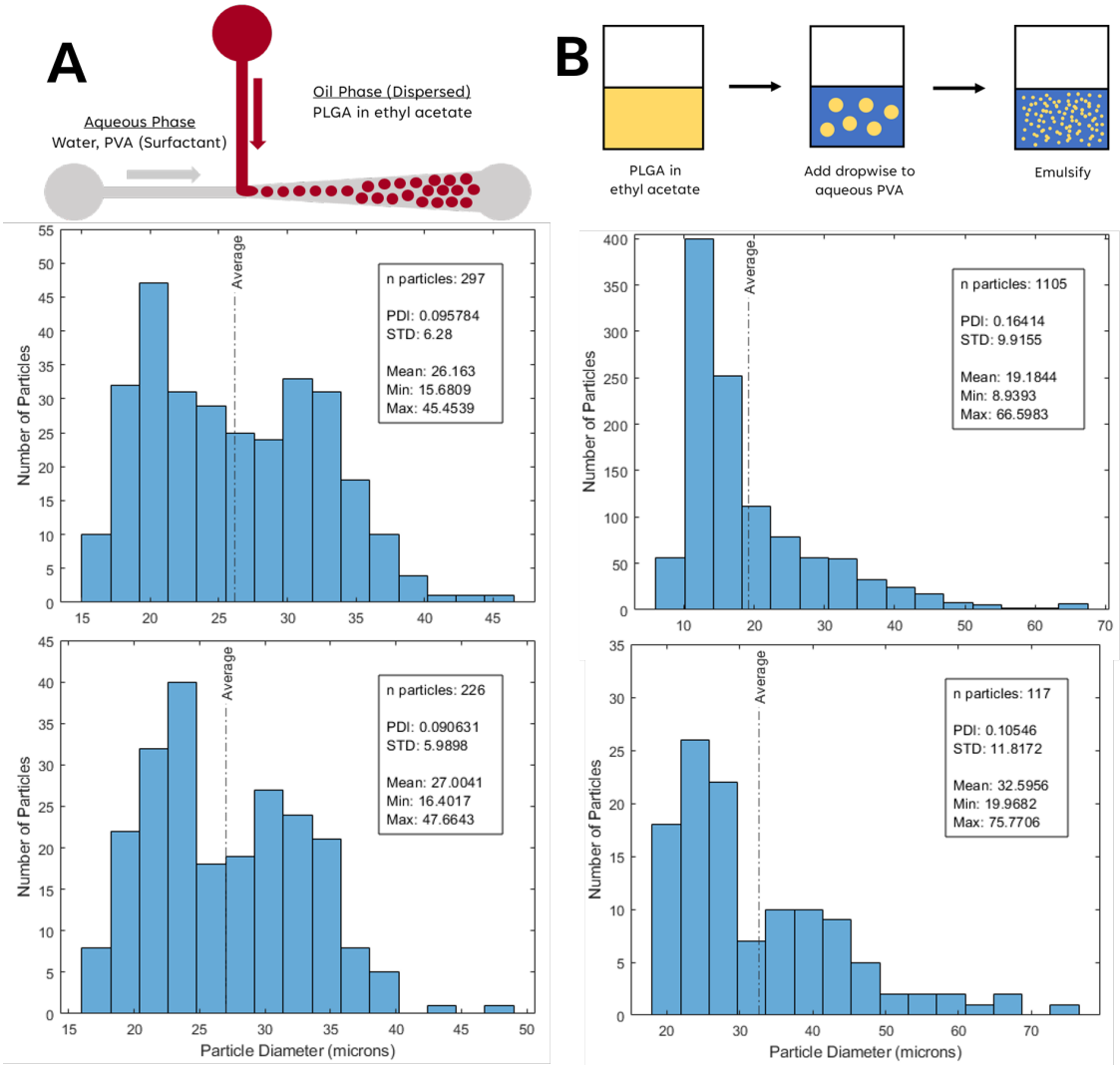

Figure 19: Comparison of consistency between batches produced by **(A)** microfluidic and **(B)** bulk emulsion techniques.

4.4 Discussion

Droplet microfluidics technology has the potential the increase the therapeutic efficacy of polymeric microparticle drug delivery systems. Specifically for this system, these results demonstrate the device fabricated via the methods discussed in Chapter 3 can successfully manufacture microparticles via emulsion droplet generation, and the resulting particles are more monodisperse than the benchtop counterparts. However, more optimization is required for this system to be translated from PLGA to more therapeutically relevant and environmentally

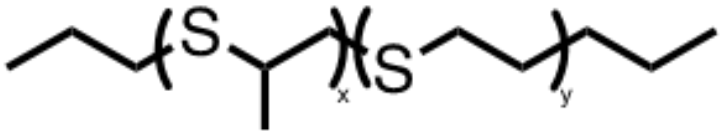

Figure 20: Chemical structure of the polypropylene sulfide (x) and ethylene sulfide (y) co-polymer (PPSES).

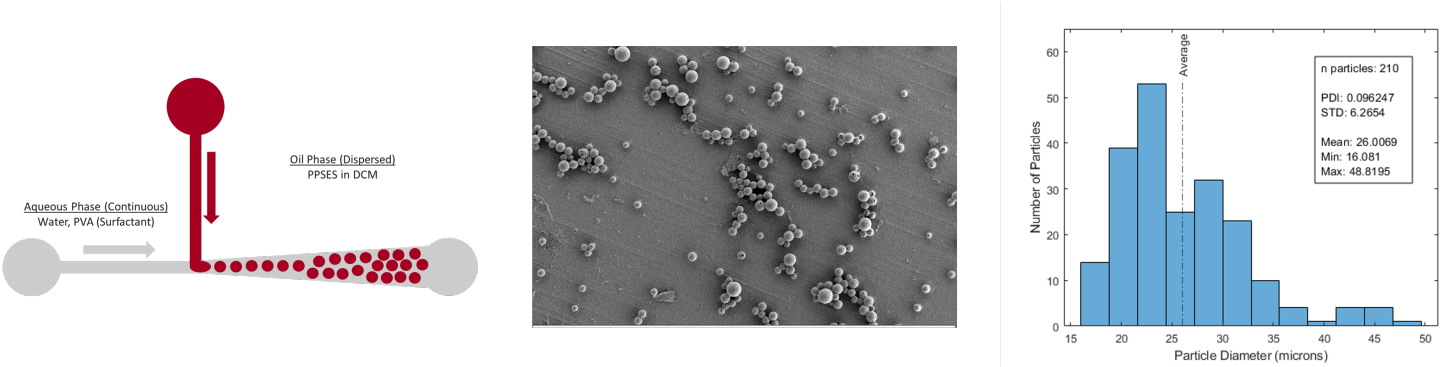

Figure 21: Microfluidic generation of 60/40 PPSES microparticles and the resulting image analysis

responsive polymeric drug delivery strategies.

Many challenges arose with the attempts to produce microparticles using PPSES. The solvents required to dissolve these were significantly more aggressive. The desire to manufacture this device in-house led to some compromises in terms of producing the most versatile and solvent compatible device possible, most notably in the capping step. PDMS, as previously discussed, is incompatible with organic solvents, and was a large source of problems when it came to trying to produce polysulfide droplets, which required aggressive solvents. Even ethyl acetate, to a lesser degree, will affect PDMS [12].

These solvents, along with the cargo they are carrying, will enter the PDMS, which is problematic for multiple reasons. This causes PDMS to swell, which did not seem to cause many problems in these short experiments, although if experiments were running for longer, swelling could eventually cause delamination[48]. The larger problem is that the cargo in the solvent leach into the PDMS with the solvent, causing material loss. Additionally, the leaching of solvent

results in a change in polymer concentration during the formulation, which caused precipitation of the polymer, thus blocking the channels. Changing polymer concentration can also have an affect on resulting particle size[49] We lowered the polymer concentration from 5% to 1% in the oil phase in an attempt to prevent this.

Polymer precipitate also makes the devices difficult to clean, as aggressive solvents cannot be used to flush the channels, and PDMS contamination can be transferred from one batch to another. This was solved by changing the PDMS between experiments, necessitating repeat surface coatings.

To fine tune the surface chemistry of the channels, many different coatings were attempted. The first attempt was to use polyethylene glycol (PEG). This was expected to increase surface hydrophilicity, and thus promote droplet formation of the oil phase as it is a very hydrophilic molecule. However, PEG is also very soluble in DCM, promoting interaction with the walls of the device from both phases, which is what was seen in the flow profile. This result led to the decision to try APTES. This was initially successful, and produced PPSES droplets. However, repeat APTES treatments due to the need to change the PDMS increased the likelihood of APTES condensation like that shown in Figure 17 C. Re-treatment allowed for interaction with preexisting nucleation sites on the surface for the molecule to self-condense. Other groups have found the same problem when coating microchannels, and report using ammonia to remove APTES[50], however this was in PDMS only devices, not glass devices. Ammonia treatment did not remove deposits from our channels. Another common hydrophilic modification in the literature for PDMS devices is the deposition of PVA in the channels[51]. This helped promote droplet formation, however, since it is only a physical adsorption of PVA onto the surface, and not covalently bonded like the silanization methods, this was not the treatment used for the final PLGA experiments. The zwitterionic silane polymer was the best choice for surface treatments, as it allows for the functionalization of channels in-situ, without any risk of self-condensation. The zwitterionic monomer is also incredibly hydrophilic, which promoted droplet formation very well. This is a novel polymer with the potential to be used in other oil-in-water droplet

microfluidics applications.

Many of these problems could have been solved with a successful glass bonding method, however this proved to be incredibly challenging with the tools at our disposal. The first method of using an adhesive, although common in the literature for slightly different applications[52], proved to be difficult given the design requirements for our application. (1) The material needed to have a low enough viscosity to spin coat very thin layers (approximately below 5 μm) such that the material did not clog the channels. There were many adhesives that met this criteria. However the material also needed to (2) have low outgassing such that during the curing process, the solvent evaporating from the polymer does not cause air bubbles, and thus leaks in the device. NASA has a certification process for materials for this purpose, and many meet this criteria individually. However, the material also needed to be (3) solvent resistant to DCM so that the bondline did not get etched away during experimentation. There was only one adhesive that was tested and certified for this, and it was quite viscous and could not be spun coat. Polyimide, the adhesive chosen for initial testing, is often sold as a film (Kapton) for taping, and this is reported by the manufacturer to be DCM resistant, however, it has a significant amount of outgassing, and therefore caused leaks.

Thermal bonding also proved to be difficult, as the glass transition temperature of borosilicate is quite high, and needed to be reached quite slowly in order to avoid cracking. Therefore, a programmable oven that reaches temperatures of around 600°C is necessary[53]. There was only one of those in-house, which was a tube furnace. Unfortunately, the way this heats the sample is via near-infrared light, which glass is transparent to. This means the heat transfer mechanism of the oven does not directly induce changes in temperature into the sample. Only by physical contact to other surfaces was it able to absorb heat, which caused it to fracture due to internal stresses. The literature on glass bonding uses more traditional atmospheric ovens that use convection as the heat transfer mechanism[33], which was not available. Others use a vacuum wafer bonder to apply specific pressure and temperature, yielding very high quality chips[54,55]. This was ruled out as a viable method after attempting very high temperatures with very slow ramp times, along with a

variety of surface treatments and weights to apply pressure. Some have suggested using plasma treatments, piranha solution, or HCl[56,57] to prime the surfaces for thermal bonding, but these all proved ineffective as well. Occasionally, when removing the slides from the oven, they would feel bonded, and would be difficult to separate, but once fluid was flown into the channels, they slide apart, suggesting these were transient Van der Waals forces holding the two together, not a true covalent or glass bonding. Given the success rates in the literature, and the only difference being the type of oven, the conclusion was that thermal bonding is not possible in-house.

4.5 Conclusion

Overall, we were able to successfully take a microfabricated glass microfluidic chip and seal it. From there, the channels were activated and made hydrophilic to promote oil-in-water droplet formation. This successfully and consistently produced PLGA polymeric microparticles, which demonstrated better quality metrics over the benchtop counterpart. These results suggest that, with some optimization, these devices can manufacture microparticles with novel, more intelligent polymers, and drug loading to improve clinical relevance.

Chapter 5

Future Directions

5.1 Concerns, Limitations, and Future Directions

Although the recipe for microfabrication of these devices is well optimized, the design proper is not. Given that a device with more defects was able to manufacture polysulfide microparticles, but the flatter were not, the defects in the device could have promoted droplet formation, and that the design may need some optimization. Even simply decreasing the width of the oil phase inlet channel has been shown to help promote droplet formation, e.g. designing the widths of the continuous phase (water) and the dispersed phase (oil) to be 50 and 20 µm, respectively[58]. Additionally, a redesign of this device could benefit from even larger inlet holes to allow for more room for error in the bonding, as well as a shorter oil inlet channel to minimized the amount of interaction with the PDMS.

This design, and the use of PDMS, may also be contributing to the inconsistency of particle production with more aggressive solvents. PDMS upon exposure to organic solvents becomes hydrophobic, which would reduce promotion of O/W droplet formation. T-junctions tend to have this problem, whereas flow focusing devices can avoid this[4], as the oil phase does not come into contact with the walls of the device at or beyond the junction. Therefore, this would be a promising next step for redesigning the channel geometry.

Additionally, there was no confirmation that any of the surface coating were present, and no investigation was done into the degree at which each one affected the hydrophilicity of the surface. We used droplet formation as a proxy for determining hydrophilicity and confirming surface coatings were successful. Additionally, it is unconfirmed that the polymeric zwitter silane modifies the surface to be more hydrophilic than an non-polymerized zwitter silane[59]. This can be investigated more robustly with NMR, AFM[59], or SEM elemental analysis. The degree of hydrophilicity can be quantified, and thus optimized, using a contact angle test. This will better

inform the decision of which surface coating to use based on which is the most hydrophilic, or even oleophobicity with the oil phase.

Throughout the duration of the microfluidic droplet generation experiments, droplet size would gradually decrease over time. Since flow rate ratio governs droplet formation, this suggests that that the flow rate of the oil phase is increasing over time. This is due to pressure building up in the system, which has been confirmed by pulling the tubing from the device and seeing a large amount of volume of the oil phase leave the tubing. Buildup of pressure means the flow rates in the device are not what are being programmed. This can be due to there being a maximum flow rate due to a general resistance to flow in the device, causing pressure to build up. Pressure may also be building up because of the volatile nature of the solvents used.

To address the pressure build-up issue, a pressure-based pumping system can be used instead of a flow rate- based system. This will better account for both back pressure from device, as well as vapor pressure from the solvents. If the two phases are experiencing a consistent pressure being applied, it can be assumed the flow rate will be consistent as well. There are many of these systems in use at Vanderbilt, including one in the VINSE cleanroom.

Given the device appeared compatible with ethyl acetate, but the polymer of interest requires a more aggressive solvent, a potential solution would be to find a chemical modification that allows the polymer to retain its crystallinity but improve its solubility in ethyl acetate. We are currently exploring variations which incorporate phenyl side chains, which allow for pi-pi interactions between the chains.

The hardening protocol in this experiment was different between the benchtop and the microfluidic formulations. Microfluidic particles entered the hardening solution as they left the device over the course of about 40 minutes, and once the experiment was over, the 10-minute timer began. This means particles in these batches are experiencing varied amount of time in the hardening solution. Although this probably did not affect the results of this experiment, when there is drug product, the hardening time should be minimized to avoid loss of drug into the solution. To resolve this, a potential new design can be a more parallelized version of the current

device such that they same number of reagents can be processed more quickly. Hardening can be done in-situ by designing in a long path for the solvent to diffuse out from. This also begs the question of how this system affects drug encapsulation efficiency and weight percent of drug, which is an immediately necessary next step in validating this system, although these are expected to improve as well.

5.2 Broader Impacts

When fully optimized, an in-house pipeline for fabricating glass droplet microfluidic devices will allow for the production of polymeric microparticle with very precise size ranges, high encapsulation efficiencies, and high drug loading. This should be compatible with a variety of polymers and small molecule drugs, and can be potentially be combined with creative drug encapsulation methods like a solid-in-oil-in water technique to encapsulate protein and siRNA cargo. Using the device without tuning the hydrophilicity can even be leveraged to make W/O emulsions for hydrogel microparticle drugs. In general, incorporating microfluidics into a workflow will allow members of the lab to more precisely fine tune the release profiles and retention times for reactive oxygen species responsive drug delivery vehicles, and more generally polymeric microparticles that target localized chronic diseases like osteoarthritis or glaucoma, making the therapeutics more clinically relevant, translational, and ultimately improving patient outcomes.

Chapter 6

Conclusions

Glass as a substrate is a robust material for microfluidics, but etching to a depth of 50 μm for the purposes of producing large polymeric microparticles is difficult to do consistently and effectively. By combining a simple negative resist lift-off layer, thick gold hard masking with a Cr adhesion layer, and a buffered HF etching system, we developed an in-house, simple, alignment-free, resist-free hard masking protocol to microfabricate high-quality, glass microfluidic device fabrication. Off target etching and channel wall defects were minimized, and surface roughness was improved by three orders of magnitude, while reaching the target depth and aspect ratio. This device was effectively sealed, and the channels were activated and made hydrophilic to promote oil-in-water droplet formation. This successfully and consistently produced PLGA polymeric microparticles, which demonstrated better quality metrics over the benchtop counterpart. These results suggest that, with some optimization, these devices can manufacture microparticles with novel, more intelligent polymers, and drug loading to improve clinical relevance.

Bibliography

[1] Carlisle R. DeJulius, Shubham Gulati, Karen A. Hasty, Leslie J. Crofford, and Craig L. Duvall. Recent Advances in Clinical Translation of Intra-Articular Osteoarthritis Drug Delivery Systems. *Advanced Therapeutics*, 4(1):2000088, 2021.

[2] Julia Paik, Sean T. Duggan, and Susan J. Keam. Triamcinolone Acetonide Extended-Release: A Review in Osteoarthritis Pain of the Knee. *Drugs*, 79(4):455, 3 2019.

[3] Moon Suk Kim, Hyun Hee Ahn, Yu Na Shin, Mi Hee Cho, Gilson Khang, and Hai Bang Lee. An in vivo study of the host tissue response to subcutaneous implantation of PLGA- and/or porcine small intestinal submucosa-based scaffolds. *Biomaterials*, 28(34):5137–5143, 12 2007.

[4] James M. Anderson and Matthew S. Shive. Biodegradation and biocompatibility of PLA and PLGA microspheres. *Advanced Drug Delivery Reviews*, 64(SUPPL.):72–82, 12 2012.

[5] C. R. DeJulius, A. Bernardo-Colón, S. Naguib, J. R. Backstrom, T. Kavanaugh, M. K. Gupta, C. L. Duvall, and T. S. Rex. Microsphere antioxidant and sustained erythropoietin-R76E release functions cooperate to reduce traumatic optic neuropathy. *Journal of Controlled Release*, 329:762–773, 1 2021.

[6] Kristin M. Poole, Christopher E. Nelson, Rucha V. Joshi, John R. Martin, Mukesh K. Gupta, Skylar C. Haws, Taylor E. Kavanaugh, Melissa C. Skala, and Craig L. Duvall. ROS-Responsive Microspheres for On Demand Antioxidant Therapy in a Model of Diabetic Peripheral Arterial Disease. *Biomaterials*, 41:166, 2 2015.

[7] Wen Li, Liyuan Zhang, Xuehui Ge, Biyi Xu, Weixia Zhang, Liangliang Qu, Chang Hyung Choi, Jianhong Xu, Afang Zhang, Hyomin Lee, and David A. Weitz. Microfluidic fabrication of microparticles for biomedical applications, 8 2018.

[8] Jianmei Wang, Yan Li, Xueying Wang, Jianchun Wang, Hanmei Tian, Pei Zhao, Ye Tian, Yeming Gu, Liqiu Wang, and Chengyang Wang. Droplet microfluidics for the production of microparticles and nanoparticles. *Micromachines*, 8(1):1–23, 2017.

[9] Qiaobing Xu, Michinao Hashimoto, Tram T Dang, Todd Hoare, Daniel S Kohane, George M Whitesides, Robert Langer, Daniel G Anderson, and H. David. Preparation of monodisperse biodegradable polymer microparticles using a microfluidic flow-focusing device for controlled drug delivery. *Small*, 5(13):1575–1581, 2009.

[10] Dao Tong Chong, Xin Shi Liu, Hua Jie Ma, Guo You Huang, Yu Long Han, Xing Ye Cui, Jun Jie Yan, and Feng Xu. Advances in fabricating double-emulsion droplets and their biomedical applications, 9 2015.

[11] J. Cooper McDonald and George M. Whitesides. Poly(dimethylsiloxane) as a material for fabricating microfluidic devices. *Accounts of Chemical Research*, 35(7):491–499, 2002.

[12] Jessamine Ng Lee, † Cheolmin Park, , and George M. Whitesides*. Solvent Compatibility of Poly(dimethylsiloxane)-Based Microfluidic Devices. *Analytical Chemistry*, 75(23):6544–6554, 12 2003.

[13] A R Abate, A Poitzsch, Y Hwang, J Lee, J Czerwinska, and D A Weitz. Impact of inlet channel geometry on microfluidic drop formation. *Physical Review E - Statistical, Nonlinear, and Soft Matter Physics*, 80(2), 2009.

[14] Jian Hong Xu, S. W. Li, J. Tan, and G. S. Luo. Correlations of droplet formation in T-junction microfluidic devices: From squeezing to dripping. *Microfluidics and Nanofluidics*, 5(6):711–717, 5 2008.

[15] Burak Yilmaz and Fazilet Yilmaz. Lab-on-a-Chip technology and its applications. In *Omics Technologies and Bio-engineering: Towards Improving Quality of Life*, volume 1, pages 145–153. Elsevier Inc., 1 2018.

[16] George M. Whitesides. The origins and the future of microfluidics, 7 2006.

[17] John P Wikswo. The relevance and potential roles of microphysiological systems in biology and medicine. *Exp Biol Med (Maywood)*, 239(9):1061–1072, 2014.

[18] Brent M. Kuenzi, Jisoo Park, Samson H. Fong, Kyle S. Sanchez, John Lee, Jason F. Kreisberg, Jianzhu Ma, and Trey Ideker. Predicting Drug Response and Synergy Using a Deep Learning Model of Human Cancer Cells. *Cancer Cell*, 38(5):672–684, 11 2020.

[19] Andrew J. DeMello. Control and detection of chemical reactions in microfluidic systems, 7 2006.

[20] Hacer Ezgi Karakas, Junyoung Kim, Juhee Park, Jung Min Oh, Yongjun Choi, Devrim Gozuacik, and Yoon Kyoung Cho. A microfluidic chip for screening individual cancer cells via eavesdropping on autophagy-inducing crosstalk in the stroma niche. *Scientific Reports*, 7(1):1–11, 12 2017.

[21] Goran T. Vladisavljević, Nauman Khalid, Marcos A. Neves, Takashi Kuroiwa, Mitsutoshi Nakajima, Kunihiko Uemura, Sosaku Ichikawa, and Isao Kobayashi. Industrial lab-on-a-chip: Design, applications and scale-up for drug discovery and delivery, 11 2013.

[22] Yen Ta Lu, Gaurav Prashant Pendharkar, Chung Huan Lu, Chia Ming Chang, and Cheng Hsien Liu. A microfluidic approach towards hybridoma generation for cancer immunotherapy. *Oncotarget*, 6(36):38764, 11 2015.

[23] Bryan Gorman. Module 1 Fundamentals of Su-8 Photolithography. pages 1–18, 2008.

[24] Lithography.

[25] Nam Trung Nguyen. Micromixers. *Micromixers*, 2012.

[26] Wayne M. Moreau. Prebake (Softbake). *Semiconductor Lithography*, pages 329–353, 1988.

[27] José M. Quero, Francisco Perdigones, and Carmen Aracil. Microfabrication technologies used for creating smart devices for industrial applications. *Smart Sensors and MEMS: Intelligent Sensing Devices and Microsystems for Industrial Applications: Second Edition*, pages 291–311, 1 2018.

[28] Chris A. Mack. Processing: Post-Exposure Bake. *https://doi-org.proxy.library.vanderbilt.edu/10.1117/3.665802.p7*, FG06:7–7, 1 2006.

[29] Dong Qin, Younan Xia, and George M Whitesides. Soft lithography for micro- and nanoscale patterning. *Nature Protocols*, 2010.

[30] George M. Whitesides and Abraham D. Stroock. Flexible methods for microfluidics. *Physics Today*, 54(6):42, 2001.

[31] Jessamine M.K. Ng, Irina Gitlin, Abraham D. Stroock, and George M. Whitesides. Components for integrated poly(dimethylsiloxane) microfluidic systems, 10 2002.

[32] Shantanu Bhattacharya, Arindom Datta, Jordan M. Berg, and Shubhra Gangopadhyay. Studies on surface wettability of poly(dimethyl) siloxane (PDMS) and glass under oxygen-plasma treatment and correlation with bond strength. *Journal of Microelectromechanical Systems*, 14(3):590–597, 6 2005.

[33] Yuksel Temiz, Robert D. Lovchik, Govind V. Kaigala, and Emmanuel Delamarche. Lab-on-a-chip devices: How to close and plug the lab? *Microelectronic Engineering*, 132:156–175, 1 2015.

[34] G. A.C.M. Spierings. Wet chemical etching of silicate glasses in hydrofluoric acid based solutions. *Journal of Materials Science 1993 28:23*, 28(23):6261–6273, 12 1993.

[35] Wen I. Wu, Pouya Rezai, Huan Hsuan Hsu, and P. Ravi Selvaganapathy. *Materials and methods for the microfabrication of microfluidic biomedical devices*. Elsevier Inc., 2013.

[36] Takanori Ichiki, Yoshinari Sugiyama, Takekazu Ujiie, and Yasuhiro Horiike. Deep dry etching of borosilicate glass using fluorine-based high-density plasmas for microelectromechanical system fabrication. *Journal of Vacuum Science & Technology B: Microelectronics and Nanometer Structures Processing, Measurement, and Phenomena*, 21(5):2188, 9 2003.

[37] Elisa Marchezini, Fernanda P Oliveira, Rafael Lopes, Joo-Young Jin, Sunghyun Yoo, Jae-Sung Bae, and Yong-Kweon Kim. Deep wet etching of borosilicate glass and fused silica with dehydrated AZ4330 and a Cr/Au mask. *Journal of Micromechanics and Microengineering*, 24(1):015003, 11 2013.

[38] Tao Tang, Yapeng Yuan, Yaxiaer Yalikun, Yoichiroh Hosokawa, Ming Li, and Yo Tanaka. Glass based micro total analysis systems: Materials, fabrication methods, and applications. *Sensors and Actuators B: Chemical*, 339:129859, 7 2021.

[39] Matin Golozar, Wai K. Chu, Laura D. Casto, Jeremy McCauley, Anna L. Butterworth, and Richard A. Mathies. Fabrication of high-quality glass microfluidic devices for bioanalytical and space flight applications. *MethodsX*, 7:101043, 1 2020.

[40] Victor Hägglund. Characterization of masking layers for deep wet etching in borofloat glass. *Thesis, University of Uppsala*, 2013.

[41] Kang Kang, Kum-Pyo Yoo, Se-Hwan Paek, and Nam-Ki Min. Surface Roughness Effect for PDMS Direct Bonding. *ECS Meeting Abstracts*, MA2005-02(11):436–436, 2006.

[42] Mårten Stjernström and Johan Roeraade. Method for fabrication of microfluidic systems in glass. *Journal of Micromechanics and Microengineering*, 8(1):33–38, 1998.

[43] V. K. Natrajan and K. T. Christensen. The impact of surface roughness on flow through a rectangular microchannel from the laminar to turbulent regimes. *Microfluidics and Nanofluidics*, 9(1):95–121, 7 2010.

[44] J. Kijlstra, K. Reihs, and A. Klamt. Roughness and topology of ultra-hydrophobic surfaces. In *Colloids and Surfaces A: Physicochemical and Engineering Aspects*, volume 206, pages 521–529. Elsevier, 7 2002.

[45] John M Nagarah and Daniel A Wagenaar. Ultradeep fused silica glass etching with an HF-resistant photosensitive resist for optical imaging applications. *Journal of Micromechanics and Microengineering*, 22(3), 2012.

[46] Matteo Todeschini, Alice Bastos Da Silva Fanta, Flemming Jensen, Jakob Birkedal Wagner, and Anpan Han. Influence of Ti and Cr Adhesion Layers on Ultrathin Au Films. *ACS Applied Materials and Interfaces*, 9(42):37374–37385, 2017.

[47] Alessandro Ofner, David G. Moore, Patrick A. Rühs, Pascal Schwendimann, Maximilian Eggersdorfer, Esther Amstad, David A. Weitz, and André R. Studart. High-Throughput Step Emulsification for the Production of Functional Materials Using a Glass Microfluidic Device. *Macromolecular Chemistry and Physics*, 218(2):1600472, 1 2017.

[48] Sachin S. Velankar, Victoria Lai, and Richard A. Vaia. Swelling-induced delamination causes folding of surface-tethered polymer gels. *ACS Applied Materials and Interfaces*, 4(1):24–29, 1 2012.

[49] Alexander J.C. Kuehne and David A. Weitz. Highly monodisperse conjugated polymer particles synthesized with drop-based microfluidics. *Chemical Communications*, 47(45):12379–12381, 11 2011.

[50] John H.L. Beal, Andrea Bubendorfer, Tim Kemmitt, Ingrid Hoek, and W. Mike Arnold. A rapid, inexpensive surface treatment for enhanced functionality of polydimethylsiloxane microfluidic channels. *Biomicrofluidics*, 6(3), 7 2012.

[51] Tatiana Trantidou, Yuval Elani, Edward Parsons, and Oscar Ces. Hydrophilic surface modification of PDMS for droplet microfluidics using a simple, quick, and robust method via PVA deposition. *Microsystems & Nanoengineering 2017 3:1*, 3(1):1–9, 4 2017.

[52] Yu Jen Pan and Ruey Jen Yang. A glass microfluidic chip adhesive bonding method at room temperature. *Journal of Micromechanics and Microengineering*, 16(12):2666–2672, 12 2006.

[53] Pan Mao and Jongyoon Han. Fabrication and characterization of 20 nm planar nanofluidic channels by glass-glass and glass-silicon bonding. *Lab on a Chip*, 5(8):837–844, 7 2005.

[54] Björn Renberg, Kae Sato, Takehiko Tsukahara, Kazuma Mawatari, and Takehiko Kitamori. Hands on: Thermal bonding of nano- and microfluidic chips. *Microchimica Acta*, 166(1-2):177–181, 6 2009.

[55] J. S. Mellors, V. Gorbounov, R. S. Ramsey, and J. M. Ramsey. Fully integrated glass microfluidic device for performing high-efficiency capillary electrophoresis and electrospray ionization mass spectrometry. *Analytical Chemistry*, 80(18):6881–6887, 9 2008.

[56] Koki Shoda, Minori Tanaka, Kensuke Mino, and Yutaka Kazoe. A simple low-temperature glass bonding process with surface activation by oxygen plasma for micro/nanofluidic devices. *Micromachines*, 11(9), 2020.

[57] Timo Mayer, Aleksei N. Marianov, and David W. Inglis. Comparing fusion bonding methods for glass substrates. *Materials Research Express*, 5(8):085201, 7 2018.

[58] Junyi Yao, Fan Lin, Hyun Soo Kim, and Jaewon Park. The Effect of Oil Viscosity on Droplet Generation Rate and Droplet Size in a T-Junction Microfluidic Droplet Generator. *Micromachines 2019, Vol. 10, Page 808*, 10(12):808, 11 2019.

[59] Lingxiang Wu, Zhang Guo, Sheng Meng, Wei Zhong, Qiangguo Du, and Laisheng L. Chou. Synthesis of a zwitterionic silane and its application in the surface modification of silicon-based material surfaces for improved hemocompatibility. *ACS Applied Materials and Interfaces*, 2(10):2781–2788, 10 2010.

Chapter 7

Appendix

7.1 MATLAB Image Analysis Code

```
%% Input Parameters
rmin = 10; %% in pixels (DON'T GO BELOW 6)
rmax = 50; %% in pixels
nBins = 15; %bins for histogram

%% Import + Get Scale
path = 'analyze/SEM/20220622/';
file = '20220622_bt1 nl_02.tif';
og = imread(append(path,file));

% automatically crop based on 1536 x 2048 size image
I = imcrop(og, [0 0 2048 1330]);

% get scale bar measurement and pixel length
% imtool(scale) and measure to double check
scale = imcrop(og, [ 8.51 1348.5 370 127.98]);
microns = str2double(regexp(ocr(scale,'TextLayout','Block'). ...
    Text,'\d*','Match'));
BW = edge(scale, 'canny');
[H,T,R] = hough(BW);

P  = houghpeaks(H,5,'threshold',ceil(0.3*max(H(:))));
x = T(P(:,2)); y = R(P(:,1));

lines = houghlines(BW,T,R,P,'FillGap',5,'MinLength',7);
max_len = 0;
for k = 1:length(lines)
   xy = [lines(k).point1; lines(k).point2];
   %plot(xy(:,1),xy(:,2),'LineWidth',2,'Color','green');

%    % Plot beginnings and ends of lines
%    plot(xy(1,1),xy(1,2),'x','LineWidth',2,'Color','yellow');
%    plot(xy(2,1),xy(2,2),'x','LineWidth',2,'Color','red');


   % Determine the endpoints of the longest line segment
   len = norm(lines(k).point1 - lines(k).point2);
   if ( len > max_len)
      max_len = len;
      xy_long = xy;
   end
```

```
end

%plot longest line for verification
%plot(xy_long(:,1),xy_long(:,2),'LineWidth',2,'Color','cyan');

pix_per_micron = max_len/microns;

%% Find circles

% Increase sensitiivity
[centers, radii_pix, metric_pix] = imfindcircles(I,[rmin rmax] ...
    ,"Sensitivity",.9);
% Show images
figure
subplot(1,3,1), imshow(og);
subplot(1,3,2), imshow(I);
subplot(1,3,3), imshow(og);
viscircles(centers, radii_pix,'EdgeColor','b'); %circles

figure
imshow(og);
viscircles(centers, radii_pix,'EdgeColor','b'); %circles

%% Stats
radii = radii_pix/pix_per_micron;
diam = radii * 2;
avgD = mean(diam);
PDI = sqrt(std(diam)) / mean(diam);

%% Plot
figure
h = histogram(diam,nBins);
hold on
yax = ylim;
ylim([0 yax(2)+5])
annotation('textbox',[.65 .65 .2 .2],'String',{'n particles: '+ ...
    string(length(diam)),'','PDI: ' + string(PDI), 'STD: ' ...
    + string(std(diam)), '    ', 'Mean: ' + string(avgD), 'Min: ' ...
    + string(min(diam)), 'Max: ' + string ...
    (max(diam)) },'FitBoxToText','on');
xlabel('Particle Diameter (microns)')
xl = xline(mean(diam), '-.', 'Average');
xl.LabelVerticalAlignment = 'top';
xl.LabelHorizontalAlignment = 'center';
```